UNIVERSITY OF CALIFORNIA,
IRVINE

Reconfigurable Reflectarray Antenna with Beam Steering Based on Metasurface

THESIS

submitted in partial satisfaction of the requirements
for the degree of

MASTER OF SCIENCE

in Electrical Engineering

by

Feiyu Shan

Thesis Committee:
Professor Filippo Capolino, Chair
Professor Lee Swindlehurst
Professor Ender Ayanoglu

2022

DEDICATION

I would like to dedicate my thesis

to my parents and my girlfriend

without whom none of my success would be possible

TABLE OF CONTENTS

LIST OF FIGURES

LIST OF TABLES

ACKNOWLEDGMENTS

I would like to acknowledge my supervisor, Professor Filippo Capolino, who made this work possible by giving me the opportunity to do research in electromagnetism. His guidance and advice have inspired me throughout me through all the stages of my project.

I would also like to thank my committee members, Professor Lee Swindlehurst and Professor Ender Ayanoglu for their assistance, support and insightful suggestions.

Special thanks to my labmates David Hanna and Miguel Saavedra Melo, for their encouragement and guidance. Without their selfless sharing, the research project wouldn't have been successful.

ABSTRACT OF THE THESIS

Reconfigurable Reflectarray Antenna with Beam Steering Based on Metasurface

By

Feiyu Shan

Master of Science in Electrical Engineering

University of California, Irvine, 2022

Professor Filippo Capolino, Chair

A reconfigurable reflectarray antenna with beam steering is presented in the thesis. The reflectarray system includes a reconfigurable reflecting surface and a feed antenna. The reflecting surface of the reflectarray antenna is composed of a periodic arrangement of unit cell elements where each cell has an embedded varactor for reconfigurability. The capacitance of varactors varies with the applied reverse bias voltage and it is used to control the phase distribution on the reflecting surface for realizing a reconfigurable system. By tuning the capacitance of the varactors, a reflected-phase tuning range of 300° is achieved by the proposed reflectarray element. The feed antenna of the reflectarray system is designed using a microstrip patch antenna with air gap included to increase the gain. The feed antenna has maximum gain of 9.8 dB and the main beam is set to be directed at the reflecting surface center. A mathematical method for feed radiation model is presented to analyze the aperture efficiency and directivity of the reflectarray system. The far-field radiation pattern result is obtained from a full-wave simulation using the commercial software CST Studio Suite. We demonstrate that the reflectarray system generates beam radiation along three different directions, as a proof of beam steering capability. The Full-wave result of the far-field simulations show that the maximum directivity is 18.5 dB which agrees favorably with the theoretical analysis.

Chapter 1

Introduction

1.1 Background of Research Topic

Nowadays among the different kinds of rapidly evolving modern technology., the development of wireless communication field is particularly prominent considering that various communication terminals have been integrated into people's daily life, such as mobile phones, broadcast TV and various smart home devices. In a wireless communication system, the antenna is essentially a transducer as a transmitter and receiver of electromagnetic waves, which can convert the guided waves from the circuit into electromagnetic waves propagating in free space. One can classify functions of antennas into three aspects: transferring energy, presetting polarization of wave for transmitting and receiving and realizing radiation distribution in space which is antenna beam direction control. For versatile wireless communication applications, requirements for antennas are becoming more and more stringent, not only the basic electrical properties are required to meet the design requirements, but also the structure of antenna is required to adapt to diverse scenarios.

Although traditional phased array antenna can meet the requirements of high gain and

multi-beam, the numbers of array units and corresponding RF channels are large, which cause problems such as high cost, complex integration and maintenance complexity. For a typical reflector antenna, it can focus an incident electromagnetic wave from the feed source by reflecting it in a given direction. However, the precise design of a curved surface and manufacturing difficulty limit its application. At the same time, traditional antennas with fixed radiation properties such as beam direction can not give solution to the future development of wireless communication. In recent years, with the development of the electromagnetic metamaterials theory, using 2D electromagnetic metamaterials or metasurfaces to design reflector antennas can reach same radiation properties as traditional reflector antennas. Also, the advantages of easy-manufacturing and small size make it more attractive. On the basis of the theory of metamaterials and metasurfaces, people have integrated periodic array elements and tunable active devices to realize reconfigurable metasurface. Reconfigurable materials such as liquid crystal materials [1, 2], varactor diodes [3, 4], RF-MEMS technology [5, 6], and PIN diodes [7, 8] can be integrated to change the properties, for example the phase, of the reflected or transmitted wave.

1.2 Overview of a Metasurface

Matematerials are composed of periodic subwavelength metallic/dielectric structures that resonantly couple to the electric and magnetic fields of the incident electromagnetic waves. The electric and magnetic resonance occur due to the interaction of electromagnetic waves and subwavelength structure. This typical phenomenon within the context of the electromagnetic domain results in unprecedented properties. The unconventional geometry and size of design in metamaterials give them a capability to manipulate electromagnetic waves which is beyond applications of conventional materials. While matematerials have attractive properties with optical and electromagnetic waves, the difficulty in the fabrica-

tion of nanoscale 3D structure and high loss of complicated geometry limit its application. One solution to the limitation of the conventional matematerials is using 2D metamaterials or metasurfaces(MS) which exhibit all of the properties of matematerials but with much simpler structure and fabrication process. MS can be fabricated using standard lithography and nanoimprinting methods which can make it low-cost and easy to fabricate. MS is used in many electromagnetic applications because of its performance for electromagnetic wave control including reflecting, blocking, absorbing [9], enhancing, and bending waves [10]. With attractive properties and simple structure, MS is used in different kinds of fields like wave-front shaping [11, 12], polarization conversion[13, 14] and radiation control or energy concentration[15, 16]. In this thesis, the electromagnetic MS is discussed and used for reflecting surface in reflectarray antenna system. The beam steering is realized based on the property of phase shifting on the reflecting surface.

In 1960s former Soviet Union researcher Veselago [17] creatively proposed that with both the dielectric constant and permeability negative, the characteristic of negative refractive index can be realized, which is a characteristic that does not exist in the natural material. Early designs of MS were mainly composed of periodic units with the same structure such as frequency selective surface (FSS) [18], electromagnetic band-gap (EBG) [19], polarization gate [20], artificial magnetic conductors [21], etc.

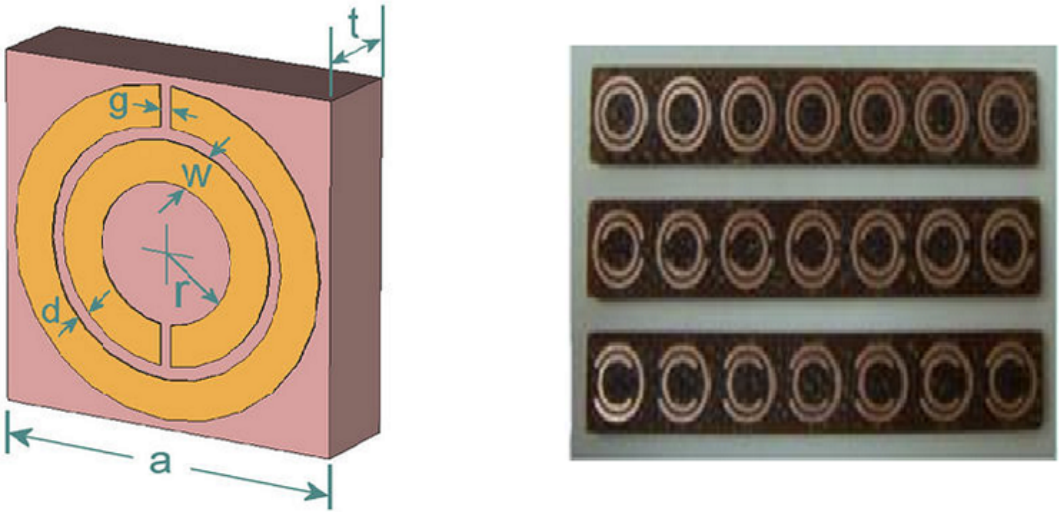

Figure 1.1: Split ring resonators (SRRs) and array structure [23].

When the electromagnetic wave travels in the periodic split resonator rings, as shown in Fig 1.1 [22]. it resonates with the magnetic field component which results in the equivalent permeability of the material becoming negative. With the development of MS research, MS modulation technologies have been proposed in recent years. By modulating the physical parameters of the metamaterial unit, one can control the electromagnetic beam pointing, polarization states and transmission modes, this kind of modulated MS demonstrates its potential in antenna design and wireless communication applications. Over the past two decades, metasurfaces have been employed for the design and fabrication of optical elements and systems. This is because its abilities have surpassed the performance of conventional diffractive optical elements. In 2019, Stefano Maci [23] applied multi-feed technology to a MS antenna realizing multi-beam, multi-polarization and beam scanning characteristics. David R. Smith [24] applied a kind of dynamic MS antenna to massive MIMO communication system for the solutions to the cost, power consumption and other problems faced by the current Massive MIMO antenna. During the past years, electronically tuning MS caught people's attention. The electronically tuned MS is able to change the working state of the unit cell element by loading active devices such as PIN diodes, MEMS switches or varactor diodes in the MS (metamaterial). Based on that, one can use the FPGA circuit system to

control the modulation state of the MS antenna in real time, thereby realize the control of the MS. In 2014, Cui [25] proposed the electromagnetic encoding and programmable MS, the states of the unit cells are represented by a combination of binary values [26, 27]. He showed states control of unit cells by loading active devices such as PIN diodes. Further using hardware systems such as FPGA to control the coding states of the digital MS in real time in order to perform dynamic control of the antenna radiation pattern.

1.3 Overview of Reflectarray

Communication over long distances attracts lots of interests with the development of wireless communication transmitter and receiver. One of the requirements in long distance communication is using large antennas in order to establish the wireless link between the transmitter and receiver. Reflector technology was first used to design telescopes [28] and applied to the field of optics to increase the observation distance. Later, it was applied in electromagnetism to control the direction of electromagnetic radiation. A typical kind of reflector antenna is parabolic reflector antenna, it consists of a circular parabolic reflector and a feed source located at the focal point of the reflector as shown in Fig 1.2. The most important property of parabolic reflector antenna is large-diameter surface which can form a highly directional beam through the reflection of the parabolic reflective surface, and then effectively enhance the main beam radiation and reduce side lobes. However, the manufacturing difficulty of the parabolic reflector antenna due to its curved surface and precise structure limit its application to large aperture antenna applications. In recent years, the requirements of low mass and cost features in antenna system design become more interesting.

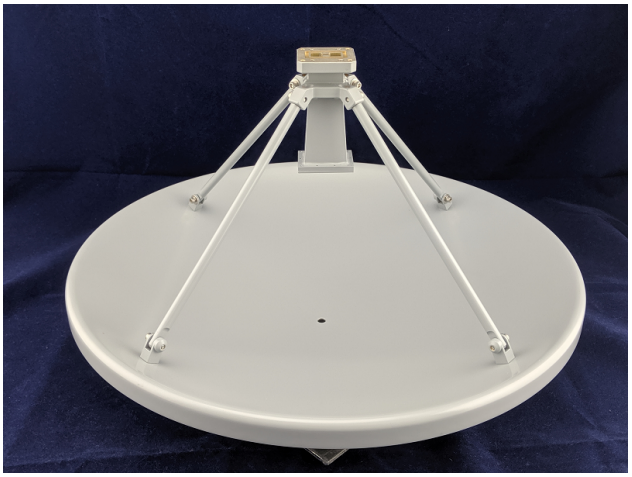

Figure 1.2: A typical 6-18 GHz parabolic reflector antenna.

An alternative approach to realize a large antenna is by using a set of small antennas to form an array which can play the same role as reflectors. The reflectarray is an antenna with a flat reflecting surface composing of hundreds of unit cell elements and an illuminating feed antenna. Planar reflectarray antenna combines the characteristics of parabolic antenna and microstrip antenna. At the same time it replaces the reflecting curve surface of traditional parabolic antennas with a planar array, which is the reason called planar reflect array antenna. Compared with traditional parabolic antennas and phased array antennas, the planar reflectarray antenna has more advantages. For example, there are many advantages such as simple feed, high gain, low profile, low mass, simple manufacture and low cost. Planar reflectarray antenna composed of many unit cell elements forms a periodic array which can reflect electromagnetic wave under the illumination of the feed antenna. By tuning the reflection phase of each unit cell element on the reflecting surface, a reflecting beam in a specific direction with high gain can be obtained.

The reflectarray antennas was first introduced in the early 1960s [29] using short ended waveguide elements with variable lengths. The lengths of short ended waveguide elements are designed to form a collimated reflecting beam because the phase of the wave changes in the waveguide. However, the bulky and heavy waveguide structure was a major drawback

at that time. Until 1980s the reflectarray antenna did not receive much attention due to the limitation of material fabrication. The introduction and breakthrough of printed microstrip antenna technology [30] simplified reflectarray structure and made it attractive in versatile applications. Over the past 10 years, an increasing interest in reflectarray antenna research has been observed in both academic and industrial sectors of the antenna community. The aperture of a reflectarray antenna comprises unit cell elements arrayed in a certain area. These arranged unit cell elements are designed to collimate the main beam of the antenna by controlling the phase of the reflected wave [31]. The attractive advantages of the reflectarray antenna, particularly its low weight and low profile, which are ideally suited for space applications, combined with ease of manufacturing, good efficiency, and high gain.

Beam steering [32] is a technique for changing the direction of the main lobe of a radiation pattern as shown in Fig 1.3. Beam steering reflectarray antenna realizes controlling the radiation pattern of reflectarray by tuning the phase distribution on the reflectarray aperture. Various enabling technologies have been used in designing phase-tuned reflectarray antennas. Tuning techniques based on mechanical actuation[33, 34] which changes the physical dimension of the unit cell elements. The primary drawback of this technique arises from requisite physical displacement. In practical, the electronic devices like PIN diode, varactor diode, FET switches and MEMS are preferred to realize phase tuning. These devices are introduced in previous paragraphs of the metasurface section. In the thesis, varactor diodes are used to control the phase distribution on the surface of reflectarray.

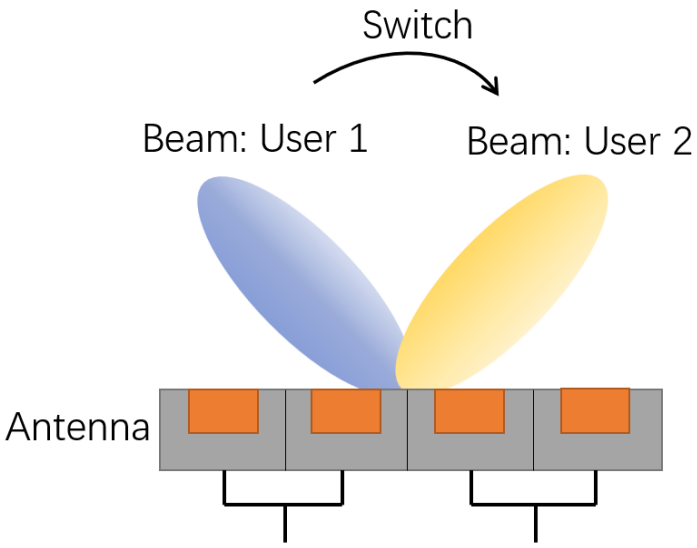

Figure 1.3: Antenna beam steering.

1.4 Outlines of Thesis

The thesis presents a kind of manufacture-friendly reflectarray and realizes reconfigurable reflecting surface for beam steering. The basis of the reflecting surface beam steering is the non-uniform phase distribution due to the phase delay when traveling in free space before intercepted by the surface. The varactor biasing is responsible for the phase shift introduced on the reflecting surface which gives the solution to the free controlling of reflecting beam direction. Also, a kind of high gain patch antenna is used as a feed antenna which is simple and low-mass compare to a conventional horn feed.

In chapter 2, the basics of a reflecting metasurface and unit cell elements design are presented. First, a conventional variable size unit cell element is analyzed to review properties of reflecting surface. Then we introduce two kinds of unit cell elements to compose metasurface which is used as reflecting surface in reflectarray system. Varactors are inserted into unit cell elements to provide the phase shift that can be controlled by reverse bias voltage.

The behavior of metasurface and unit cell are obtained from a full-wave simulation using the CST Studio Suite software by applying unit cell boundary condition for a periodic structure.

In chapter 3, the reflectarray antenna system is introduced. The theoretical analysis of reflecting beam direction is given and a center-fed symmetrical circular reflecting surface is presented. For the feed antenna in the reflectarray system, we introduce a microstrip antenna with air gap inserted to increase gain result. Besides, the effect of feed position is considered.

In chapter 4, the aperture efficiency and directivity are analyzed. Three specific efficiencies are calculated from the definition and mathematical model including the spillover, taper and blockage efficiency.

In chapter 5 the full-wave simulation results are shown, three different reflecting beam directions that $(\theta = 45°, \phi = 45°)$, $(\theta = 20°, \phi = 20°)$ and broadside are presented. The function of beam steering is satisfied and the gain result agrees with that from theoretical analysis.

Chapter 2

Design of a Metasurface and Unit Cell Element

2.1 Introduction of the Unit Cell Element

Planar reflectarray antennas rely on unit cell elements to perform phase shift. Commonly there are three types of methods used to adjust the reflection phase: elements with variable size [35], elements with variable rotation angles and elements with phase/time delay lines [36, 37]. The first method uses different electrical size of a patch to achieve phase shifting. Elements with variable rotation angles are mainly used in the design of circularly polarized antennas [38, 39]. By adjusting the rotation angle of each reflectarray unit element, it can compensate for the phase shift of the reflected beam from the unit cell to the feed antenna. The last method is to provide the phase shift of each unit cell by changing the length of the transmission line loaded at the end of the unit cell. However, traditional metasurfaces are difficult to be tuned after being fabricated, which considerably limits the degree of freedom for full-wave control. As such, it is highly desirable to realize dynamic metasurfaces, whose

functionalities can be actively tunable with controlled external methods. In contrast to the previous techniques in which static beam focusing is realized using fixed metasurfaces, reconfigurability enables dynamic beam control in scenarios where terminals are mobile.

In recent years, using tunable active devices like PIN diodes and varactor diodes has became popular in reflectarray design. The PIN diode is a special diode which can be configured as an RF switch. It enables a metasurface element to be switched between radiating (ON) and non-radiating (OFF) states, depending on the bias applied to the diodes. By this arrangement, the phase distribution of the radiated fields can be reconfigured, thereby controlling the beam direction in the far-field. For a varactor diode, it has similar function as that of PIN diode, furthermore, the linear characteristic of varactor tuning can provide smoother phase shift which is preferred in metasurface design. In this section, the unit cell element with variable size is introduced first to review the properties of the metasurface. Then the unit cell element with varactor diode is designed for reconfigurable reflectarray.

2.2 Analysis of Variable Size Unit Cell Element

Before introducing the reconfigurable reflectarray system, it is useful to analyze first the structure and performance of a traditional reflectarray because both types of reflectarray surfaces composed of array of unit cells which can provide phase shift. The properties of a traditional reflectarray can be extended to a reconfigurable reflectarray system. In this section the unit cell element with variable size is analyzed.

In this approach, the physical size of the element is changed to provide phase tuning. When incident electromagnetic wave impinges on the surface composed of sub-wavelength structure, the patch resonates at some specific frequency. Theoretically, the changing of the resonant patch size results in shifting of the resonant frequency. Therefore, the operating

principle of the variable size technique is based on the fact that reflected phase from resonant elements with different sizes would be different. The variable size technique was first introduced in [40] and [35] with crossed dipoles and rectangular patches. Square and circular patch geometry are the most common structures for conventional variable size techniques, many other kinds of geometries can be adopted as the unit cell for providing phase shift. In this thesis, we focus on the square patch geometry because of its simplicity.

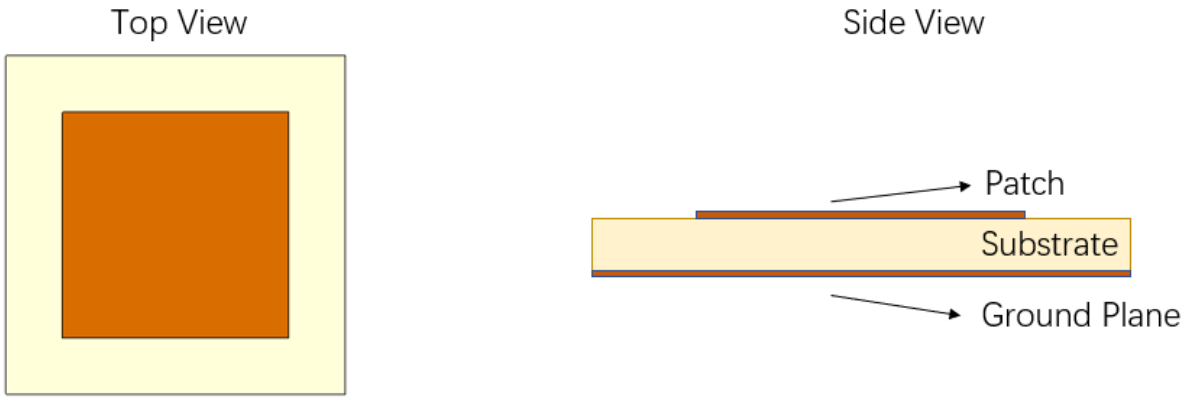

Figure 2.1: Typical square patch unit cell element.

Due to the high quality factor of the highly resonant square patch unit cell, the phase shift change in the reflected wave is highly related to structure size. Theoretically, the magnetic resonance occurred on the unit cell can provide a complete phase shift from $-180°$ to $180°$, however, the total achievable phase range which is useful to reflectarray system is around a phase cycle of $300°$ because of some effects such as substrate thickness and separation between patches. For most reflectarray system design, a phase shift cycle around $300°$ is sufficient. A typical square patch unit cell is shown in Fig 2.1. The patch is a square type and can be changed in size.

Because the resonant frequency is changing with the variation of the unit cell structure. The different phase shift in a frequency range is obtained as shown in Fig 2.2, the unit cell

provides a typical S shaped curve as the phase shift. In this case the patch size (A_{patch}) is ranged from 7mm to 14mm which provide a discrete phase distribution in a specific frequency. Because of the quality factor resonant nature of printed patches, the phase variation obtained using this approach is highly non-linear. As shown in Fig 2.2, a rapid phase variation occurred near the resonant frequency while slow variation on the two sides. In the result of this case, a 1 GHz frequency band around 6 GHz is available for reflectarray phase distribution. For example, a range of phase distribution from $-150°$ to $150°$ can be obtained at 6 GHz.

This kind of variable size technique can easily provide phase shift on the reflectarray because of the simplicity of printed patch. However, the phase distribution is fixed and non-reconfigurable which limits the application in the mobile wireless communication system. To satisfy the diversity requirement of 5G communication system, introducing varactors in the unit cell to control the phase shift gives the solution to realize a reconfigurable reflectarray system. In the next section, a unit cell element based on a dogbone-shaped structure with varactor inserted is introduced.

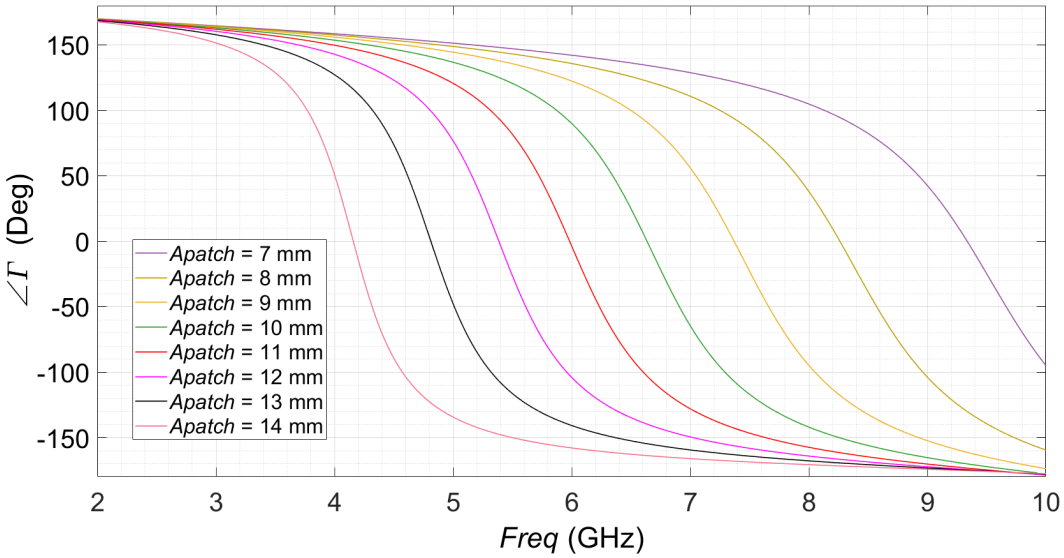

Figure 2.2: Reflection coefficient of variable size patches.

2.3 Introduction of Fat Dipole and Dogbone-shaped Unit Cell Elements

2.3.1 Fat Dipole Elements

The rectangular patch on the substrate is divided into two pieces as shown in Fig 2.3. This kind of unit cell is similar to a simple dipole antenna with two arms at two sides of the gap. For a dipole antenna, increasing its radius can obtain the result with more broadband. Therefore, this kind of unit cell element with two separated patches can be viewed as a fat dipole element.

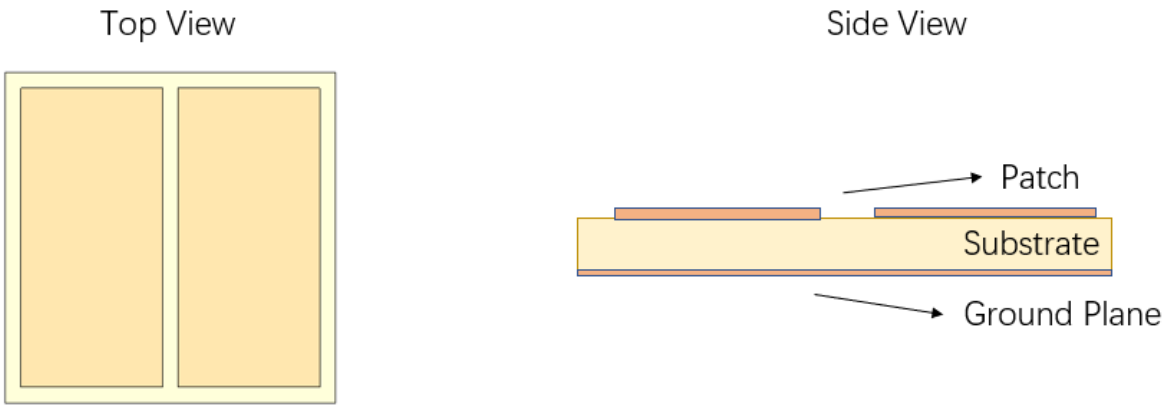

Figure 2.3: Fat dipole unit cell elements.

2.3.2 Dog-bone shaped Unit Cell Elements

The dog-bone shaped structure is introduced in [41] and has the property acting as an effective NRI (Negative Reflection Index) medium. The resonance of the dog-bone shaped unit cell is defined as magnetic resonance and electric resonance. Electric and magnetic

resonances are excited in dielectric metasurface, which can be classified as Mie resonances. This kind of resonance provides a novel mechanism for the creation of magnetic or electric resonance based on displacement current, which can replace the plasmonic resonances in metallic counterparts, and thus cause the dielectric metasurface to produce electromagnetic response, including amplitude modulation, abrupt phase jump production and so on. In dog-bone shaped unit cell, the electric resonance is associated with a dipole-like symmetric mode which creates an electric dipole moment. The magnetic resonance which is related to asymmetric mode are confined to the close proximity of the dog-bone pair and are loosely coupled to the adjacent cells. The equivalent transmission line model is given for represent pairs of planner conductors in [42]. Based on theoretical analysis of the structure, some geometry composed of periodic array of dog-bone shaped conductors are introduced like reconfigurable metasurface [43] and high impedance surface [44].

In the reflectarray system design, the magnetic resonance is responsible for introducing the phase shift. Therefore the dog-bone pair structure introduced in [45] is designed on the substrate with ground backed. As show in Fig 2.4, the half of the dog-bone pair is used as the unit cell in the reflecting surface.

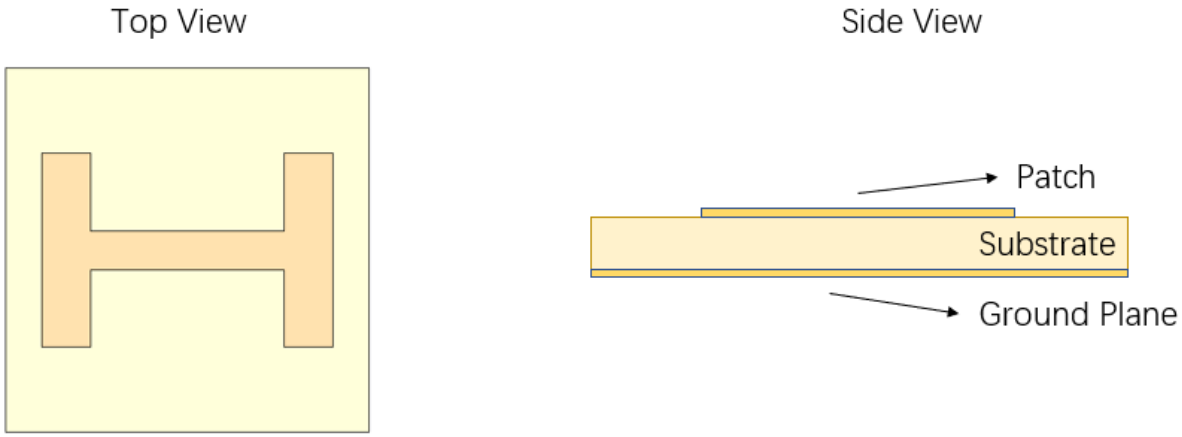

Figure 2.4: Top and back view of dogbone shaped unit cell element.

2.4 Equivalent Circuit Model of Varactor

Figure 2.5: Equivalent series RLC circuits of varactors .

Varactors are used as voltage-controlled capacitors. A DC voltage is applied as reverse bias across the varactors to alter its capacitance. In this thesis, with different structure and dielectric materials of two kinds of unit cell elements, different capacitance ranges are required. SKYWORKS SMV1231-079LF varactors are used for the fat dipole unit cell elements and MACOM MAVR-011020-1411 varactors are used for the dog-bone shaped unit cells. The relationship of total capacitance of the varactor and bias voltage is given by the datasheet from manufacturers.

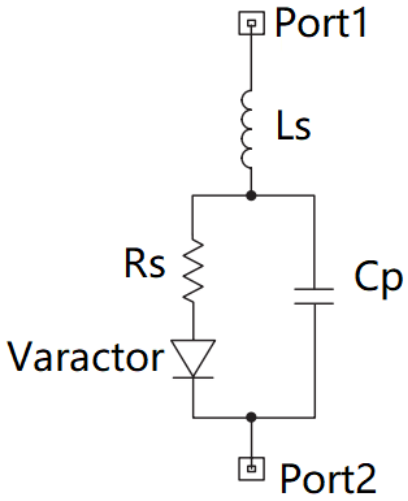

Figure 2.6: Spice model of varactors.

To use varactor diodes in full-wave simulation, the equivalent series RLC circuit model, as shown in Fig 2.5, is obtained by performing a circuit simulation in ADS software using the spice model, as shown in Fig. 2.6, and the varactor parameters for getting S-parameters

and Z-parameters in the two port network and then convert the result of two port network into RLC parameters as shown in Fig 2.7.

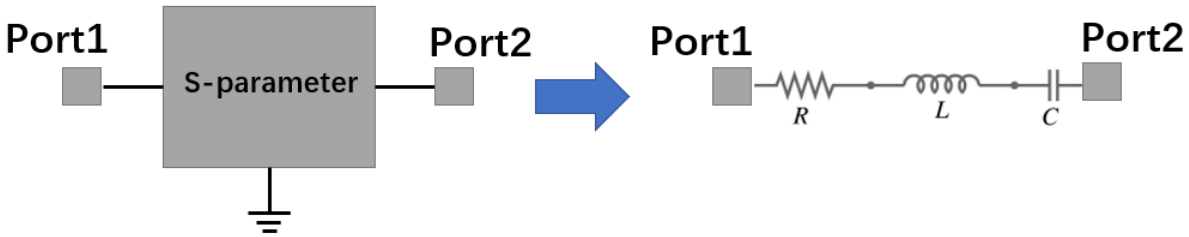

Figure 2.7: Two port network.

In the spice model, series resistance R_s, series inductance L_s and parallel capacitance C_p are from datasheets. For equivalent series circuit model, R can be obtained from the real part of Z-parameters, and L is same as Ls which is 0.7 nH. C is calculated by

$$C = \frac{1}{\omega^2 L - \omega Im(Z)} \tag{2.1}$$

where Im(Z) represents the reactance of the two port network.

The parameters of equivalent circuit of SKYWORKS SMV1231-079LF varactors are shown in Table 2.1.

Table 2.1: Values for the RLC circuit model of the SMV1231-079LF varactor

$\mathbf{V_{DC}(V)}$	$\mathbf{R(\Omega)}$	$\mathbf{L(nH)}$	$\mathbf{C(pF)}$
-10	0.037	0.7	0.501
-11	0.024	0.7	0.488
-12	0.016	0.7	0.478
-13	0.011	0.7	0.471
-14	0.007	0.7	0.465
-15	0.005	0.7	0.460

The parameters of equivalent circuit of MACOM MAVR-011020-1411 varactors are shown in Table 2.2.

Table 2.2: Values for the RLC circuit model of the MAVR-011020-1411 varactor

$\mathbf{V_{DC}(V)}$	$\mathbf{R(\Omega)}$	$\mathbf{L(nH)}$	$\mathbf{C(pF)}$
-2	2.36	0.7	0.12
-3	1.96	0.7	0.09
-4	1.77	0.7	0.075
-5	1.63	0.7	0.065
-6	1.41	0.7	0.06
-7	1.18	0.7	0.054
-8	0.88	0.7	0.045

2.5 Phase Shift Technique Using Varactor

In the reflectarray antenna design, to obtain a certain direction beam of the reflectarray, the reflecting surface has to compensate the phase delay of the wave from feed antenna and provide a progressive phase distribution which is discussed in Chapter 3. Traditional reflectarray antennas use three methods to realize phase distribution: elements with phase/time delay lines, elements with variable sizes and elements with variable rotation angles. Among the three groups of phase tuning approaches, unit cells with variable sizes is the most convenient and popular method. However, this type of phase tuning technique is non-reconfigurable which means the reflectarray is design for a fixed radiation direction, limiting the application of the reflectarray antenna. One possible way to realize a reconfigurable radiation beam is adding varactors in the unit cell to control the phase shift on the aperture.

In the thesis, varactors are inserted into the two kinds of unit cell elements to realize

the phase shift control on the reflecting surface. For fat dipole unit cell elements, varactors are located at the center of two rectangular patches as shown in Fig 2.8. This design uses RO4350B as the dielectric substrate. The structure parameters, in mm, are: A = B = 21, A1 = 1.85, A2 = 1, B1 = 2, B2 = 1, H = 1, and G = 0.4. SKYWORKS SMV1231-079LF varactor is used in this structure.

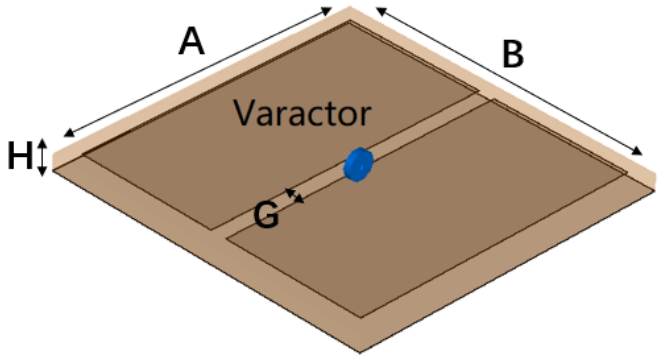

Figure 2.8: Fat dipole unit cell element with varactor.

For each unit cell, the magnetic resonance of incident wave on its surface provide phase shift of 2π. The results of phase and magnitude of reflection coefficient are shown in the Fig 2.9. With the bias voltage of varactors varying, the capacitance of varactors control the phase shift on the reflecting surface. In a specific, a phase range from π to $-\pi$ can be obtained which is useful in the reflectarray surface distribution to control the reflection beam direction.

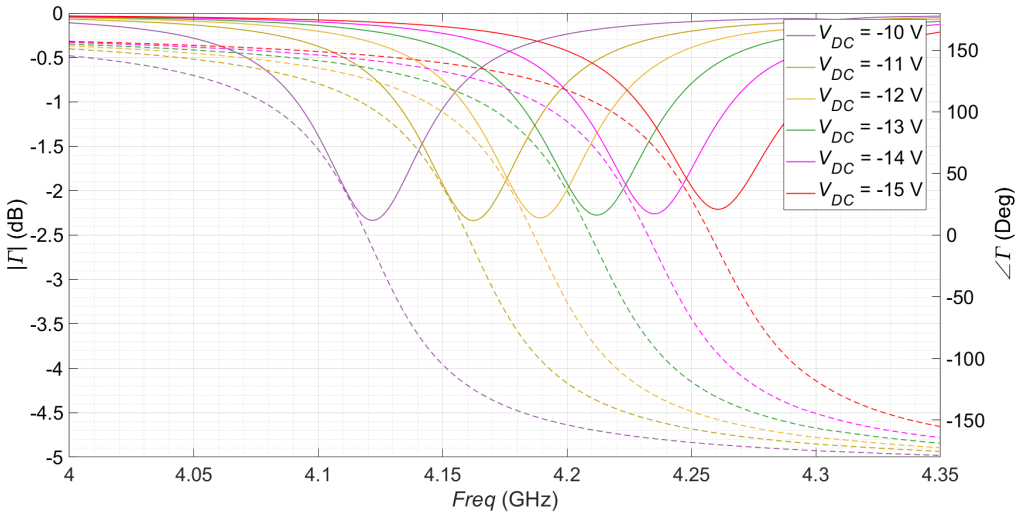

Figure 2.9: Full-wave result of magnitude and phase.

For the dog-bone unit cell element, as show in Fig 2.10, each unit cell includes two parts of dog-bone cell in reversed direction and a varactor inside the gap of two parts. This kind of geometry makes each unit cell contains one varactor, also it can be represented and analyzed by the equivalent circuit model in [42]. The performance of the dog-bone unit cells with varactors is determined by the parameters of the structure and the capacitance of the varactor. These effects including: 1. substrate inductance which is determined analytically from the dielectric substrate height and relative dielectric constant. 2. The resistance, capacitance and inductance associated with the dog-bone unit cell. 3. The varactor capacitance in parallel which is calculated for various varactor voltages from the datasheet provided by the manufacturer.

The final design of the grounded dog-bone structure considered in the thesis is shown in Fig 2.10. This design uses RT5880LZ as dielectric spacer, with relative permittivity ϵ_r = 2 and tan delta = 0.0037, and its physical dimensions, in mm, are: A = B = 15, A1 = 3, A2 = 14, B1 = 6, , B2 = 2, H = 1, and G = 1. The device used here to allow a reconfigurable behavior is a varactor diode arranged in the middle of the structure and joining the two parts of the dog-bone that are separated by the gap. MACOM MAVR-011020-1411 varactor

is used in this structure.

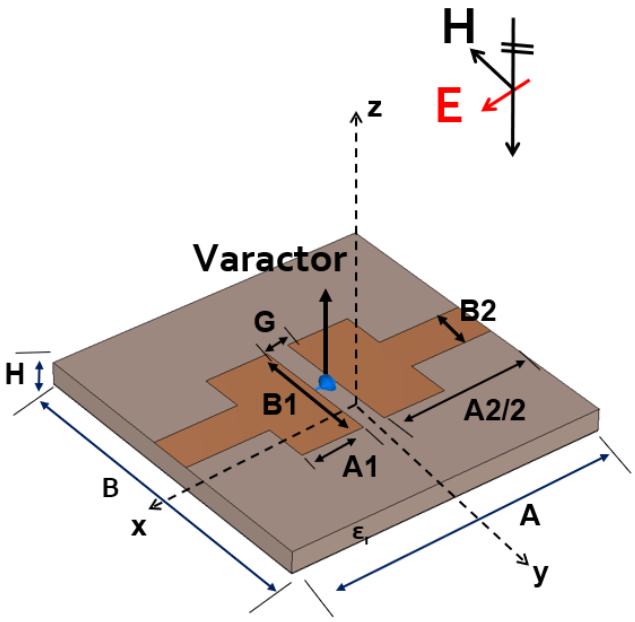

Figure 2.10: Metamaterial dog-bone unit cell with geometrical parameters.

The behaviour of the dog-bone unit cell element is same to that of fat dipole as shown in Fig 2.11. Both of these two kinds of unit cells realize the phase shifting and varactor control. In the thesis, the dog-bone unit cell with varactors is used to constructure the reflectarray system to realize the reconfigurable property and beam scanning.

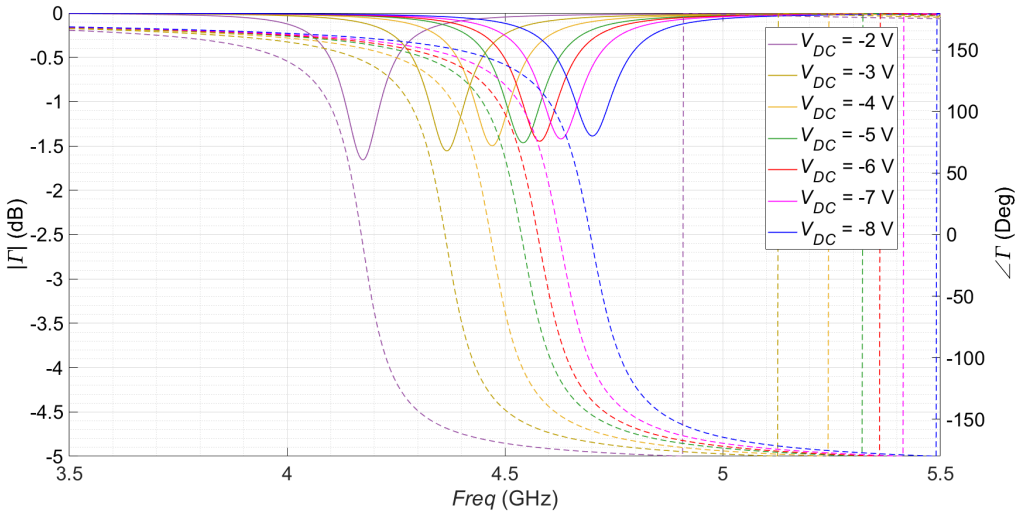

Figure 2.11: Full-wave result of S11 and phase.

2.6 Design of Metasurface

Metasurface formed by a periodic arrangement of grounded dog-bone shaped conductors on a dielectric substrate. In the full wave simulation, the unit cell boundary condition is introduced to realize the performance of the metasurface composed of the array of unit cells. The unit cell boundary condition simulate infinite elements to calculate the performance of the metasurface. As shown in Fig 2.12, the unit Cell boundary condition in CST virtually repeats the modeled structure periodically in two directions up to infinity.

In practical the reflecting surface of the system has limited numbers of unit cell elements. The result of boundary condition with infinite unit cell elements can be extended to practical surface since we focus on different unit cell elements to provide different phase distribution.

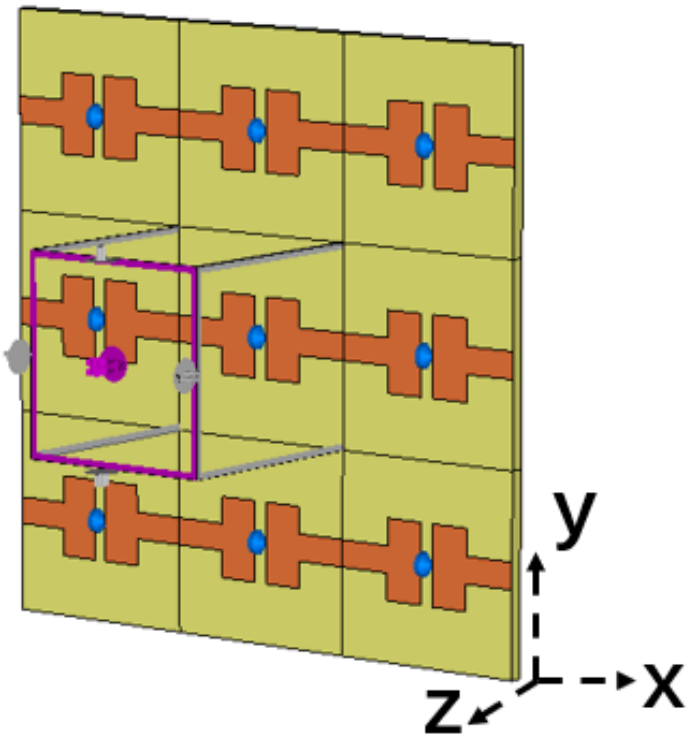

Figure 2.12: Perspective view of the metalayer formed by a periodic arrangement of grounded dogbone-shaped conductors layed on a dielectric substrate.

The relationship between phase of the reflection coefficient and the bias voltage is given in Fig 2.13. At 4.4 GHz, the phase of reflection coefficient varies from $-150°$ to $150°$ when the bias voltage decrease from -2 V to -8 V. The relationship between these two factors is non-linear, so that the phase decreases rapidly in the range of -4 V to -3 V. However, since the varactor is linear tuning, a continue phase distribution can be obtained by choosing proper bias voltage.

This relationship can be used in reflecting surface design since each unit cell element has specific phase, the related bias voltage is given to make up the total reflecting surface with a progressive phase distribution.

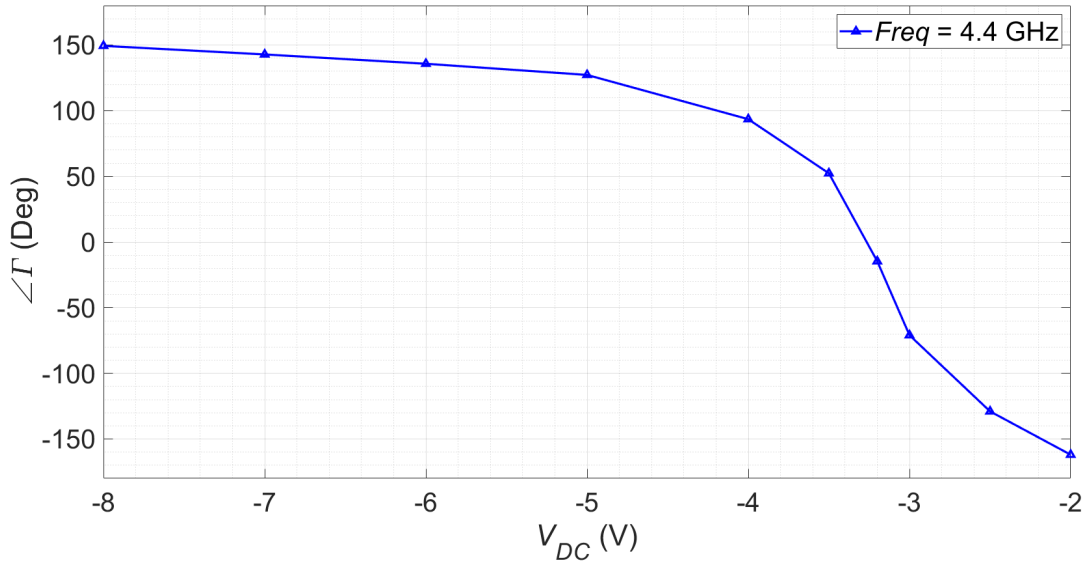

Figure 2.13: Reflection coefficient phase of the structure for biasing voltages of the varactor from -8 V to -2 V.

In the next chapter, the reflectarray system design is introduced including feed antenna characteristics and the phase distribution analysis of the system. The phase shift technique introduced in this chapter is extended to the whole system of the reflectarray antenna.

Chapter 3

Reflectarray System Design

The reflectarray system consists of an illuminating feed antenna and a flat reflecting surface with numerous elements on its aperture. The feed antenna design is introduced in this section and the planar reflecting surface is realized using metasurface and unit cell elements introduced in the previous section.

3.1 Feed Antenna Characteristic

The feed antenna radiation characteristic is one of the most important parts in a reflectarray system design. Typically a horn antenna with characteristic of moderate directivity, low standing wave ratio and broad bandwidth is used. The horn antenna is often used as feed antennas for large antenna structures such as parabolic antennas. While the horn antenna used as feed antenna is suitable to a reflectarray antenna system, the relative high cost of prototyping and complicated manufacturing process limit the performance of reflectarray system. Considering the points mentioned above, a microstrip antenna can be a suitable replacement for the horn antenna. The first microstrip antenna was proposed by Deschamps

[46] in 1953. In the next twenty years with the development of photolithographic techniques and copper clad laminate, the first microstrip antenna was manufactured and attracted researchers and industries' attentions. Microstrip antennas have been widely researched and developed over decades and numerous designs have been introduced in applications such as wireless communication, doppler radar and telemetry remote sensing, etc. The most common type of a microstrip antenna is the patch antenna which is usually employed at high frequency since the size of the patch antenna is directly relate to the wavelength at the resonant frequency. With the simple 2-dimensional structure, patch antennas are relatively inexpensive to manufacture and design compared to horn antennas. At the same time, a single microstrip patch antenna can provide a maximum gain of 10 dBi and further structural improvement can also increase the gain.

In the thesis, a C-band 4.4 GHz microstrip antenna is designed as the feed antenna of the reflectarray antenna system. The antenna performance improvement technology is introduced. For high gain and wide frequency band, we introduce a method that insert a air gap between substrates.

3.1.1 Design of Microstrip Patch Antenna

The simplest rectangular microstrip patch antenna consists of a rectangular patch, substrate material with relative dielectric constant ϵ_r and a large ground plane backed. The design of microstrip patch antenna is based on the formulas which define the structure's parameters of rectangular microstrip patch antenna. The width of the patch is given by [47, p. 469]

$$W = \frac{\lambda}{2}[\frac{\epsilon_r + 1}{2}]^{-0.5} \tag{3.1}$$

where λ is wavelength that calculated at resonant frequency. ϵ_r is dielectric constant of

the substrate.

The design formulas for the patch length is given by [47, p. 469]

$$L = 0.5\frac{\lambda}{\sqrt{\epsilon_r}} - 2\triangle L \tag{3.2}$$

where $\triangle L$ is fringing length given by [47, p. 469]

$$\triangle L = 0.412\frac{(\epsilon_{re} + 0.3)(\frac{W}{t} + 0.264)}{(\epsilon_{re} - 0.258)(\frac{W}{t} + 0.8)}t \tag{3.3}$$

where t is thickness of the substrate and ϵ_{re} is the effective dielectric constant given by [47, p. 469]

$$\epsilon_{re} = \frac{\epsilon_r + 1}{2} + \frac{\epsilon_r - 1}{2}(1 + \frac{10t}{W})^{-0.5} \tag{3.4}$$

It is the fringing fields that is responsible for the radiation. The fringing E-fields on the edge of the microstrip antenna add up in phase and produce the radiation of the microstrip antenna.

For the patch introduced in the thesis, the substrate consists of FR-4 material with dielectric constant 4.3 and thickness of 0.28 mm. The patch and ground plane layers are made of copper with thickness of 0.035 mm. The length and width of substrate and ground plane are set that the distance from their edges to patch is lambda/4 at 4.4 GHz.

Some optimization techniques of rectangular microstrip antenna are introduced in the following.

A. Coaxial Cable or Probe Feed

In this thesis the coaxial cable or probe feed method is used. The microstrip antenna is fed from underneath via a probe. The outer conductor is connected to ground plane and the inner is extended up to the patch antenna. A kind of insulator is added between the

inner and outer conductors. The advantages of this method is that the position of the feed can be altered to control the input impedance. The gain can be also improved compared to microstrip line feed method. However, the probe will also radiate, which can lead to radiation in undesirable directions.

B. Air Gap between Patch and Ground

An air gap between radiating element and ground plane is inserted to obtain a high gain and high efficiency. The air gap reduces both the electric field concentration on the lossy material and the dielectric constant of the radiating plane.

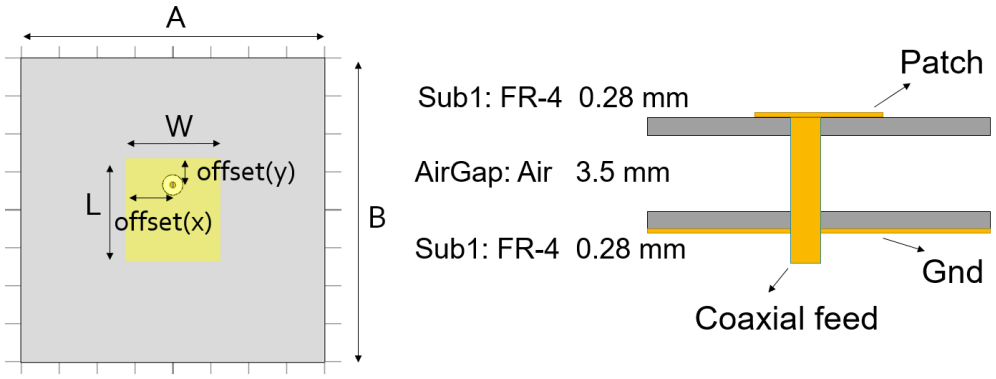

Figure 3.1: Top and side view of microstrip patch antenna.

The calculated and optimized parameters of the patch structure are shown in Fig 3.1. The copper layer under the FR4 substrate acts as the ground plane which is of 80*80 mm in dimensions, while the radiating rectangular patch of 27*25 mm is designed at the upper layer. Feeding point on The feeding point on the patch is offset from the edges W by 7 mm and L by 12.5 mm, which acts as the feeding network using microstrip probe feeding technique. The air gap is selected as 3.5mm. The simulation is based on CST software.

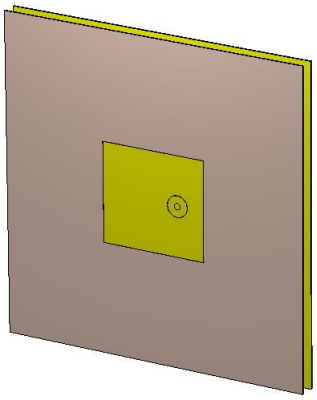

Figure 3.2: 4.4 GHz microstrip patch antenna.

By changing the position of the coaxial feed, the input impedance can be tuned easily to get a result of S11 parameters which is less than -10 dB as shown in Fig 3.3. This means that at the resonant frequency the coaxial feed matches to the patch and obtain a maximum far-field radiation.

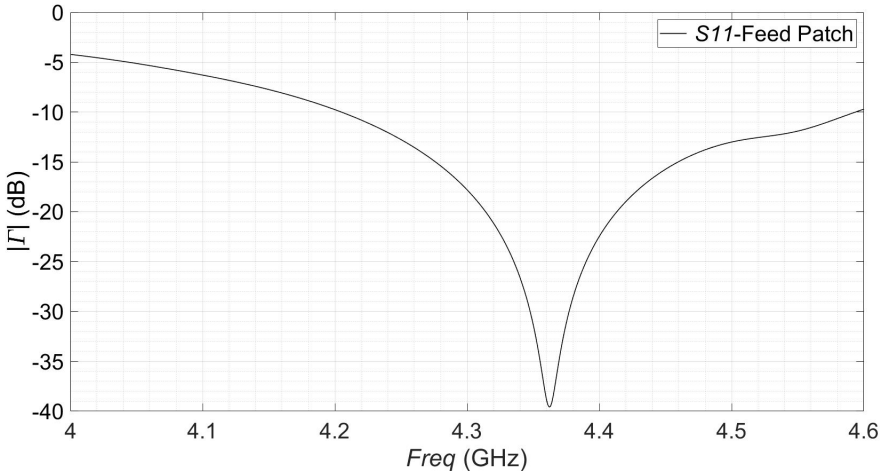

Figure 3.3: S11 parameter of patch antenna.

The result of the far-field gain of the microstrip antenna is shown in Fig 3.4. The directivity of the microstrip antenna is 9.8 dB and total losses is very low which means that there is a good input impedance match.

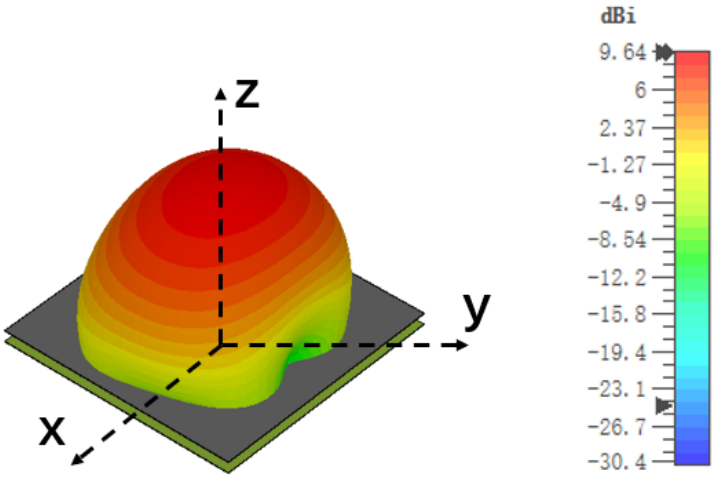

Figure 3.4: 3d far-field radiation pattern of patch antenna.

The final gain of the microstrip antenna is 9.7dB in the broadside direction along z axis vertical to the patch surface. This patch antenna is used as the feed antenna in the reflectarray system. In the next chapter, a cosine model of ideal feed antenna based on its directivity is introduced to calculate the efficiency of the reflectarray system.

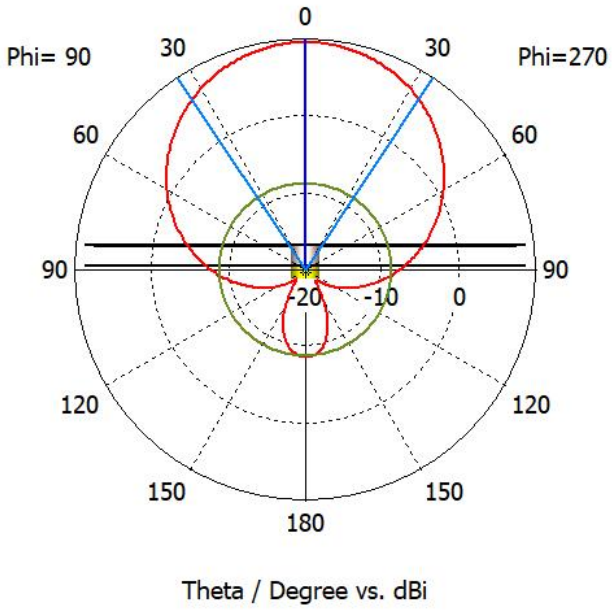

Figure 3.5: polar plot of radiation pattern.

3.2 Reflectarray System Design

The reflecting surface is made of the unit cell array which provides impedance to reflect incident electromagnetic wave. The reflecting beam direction depends on the phase distribution, in this section we analyse the relationship between the phase distribution on the reflecting surface and reflecting beam direction.

3.2.1 Phase Distribution of Reflecting Surface

For a planar antenna reflecting surface, a uniform phase distribution on the surface will yield a collimated beam in the broadside, that is, normal to the plane of the array. To control the beam reflected in a specific direction of reflectarray, the main point is to realize a progressive phase distribution on the reflecting surface which is made of unit cells with different phase. Typically, the unit cells are located in the position assumed to be far-field of the feed antenna. Therefore, the incident EM wave radiated by a feed antenna can be approximated by a plane wave that excites the unit cells with a certain incident angle. The electromagnetic wave from the feed antenna arrives on the aperture with different phase proportional to the distance from feed to each unit cell, which is referred as spatial phase delay. To obtain a certain direction of reflecting beam from reflectarray the phasing unit cells of reflectarray have to compensate for this phase. The typical geometry of a planar reflectarray is shown in the Fig 3.6.

Due to the structure of the reflectarray system and the distance from feed antenna to each unit cell. The spatial phase delay (spd) of each unit cell should compensate for can be calculated as [31, p. 65]

$$\phi_{spd} = -k_0 R_i \tag{3.5}$$

where k_0 is the wavenumber calculated in the resonant frequency. R_i is the distance from

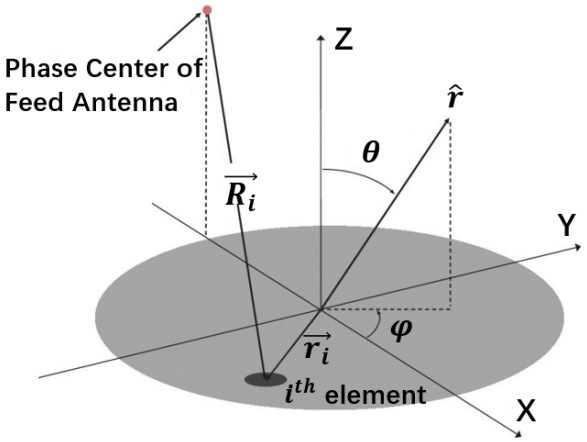

Figure 3.6: Reflectarray Geometry.

feed antenna to each unit cell. Such a phase shift provides a reflecting beam in the broadside. To realize the beam scanning in any direction in the reflectarray system, a progressive phase on the aperture is necessary. The progressive phase (pp) for each unit cell is given by [31, p. 66]

$$\phi_{pp} = -k_0 \vec{r_i} \cdot \hat{r} \tag{3.6}$$

where $\vec{r_i}$ is the position vector of the unit cell and $\hat{r}$ represents the direction of the reflecting beam. For each unit cell, its position can be represented as (x_i, y_i). Assume that reflecting beam directed in maximum direction (θ_r, ϕ_r) in the far-field. Using the definition to replace $\vec{r_i}$ and $\hat{r}$, then equation (3.6) becomes [31, p. 66]

$$\phi_{pp} = -k_0(x_i \sin\theta_r \cos\phi_r + y_i \sin\theta_r \sin\phi_r). \tag{3.7}$$

The total phase shift on the each unit cell is sum of compensation for the spatial delay ϕ_{spd} and additional progressive phase ϕ_{pp} [31, p. 66]

$$\phi_{RA} = k_0(R_i - (x_i \sin\theta_r \cos\phi_r + y_i \sin\theta_r \sin\phi_r)) + \Phi_0, \tag{3.8}$$

where Φ_0 is a phase constant. With the mathematical result of phase shift on the each

unit cell, the phase distribution of the reflecting surface can be calculated for different feed antenna positions and reflecting beam directions. As an example, the phase distribution of a C-band reflectarray antenna with a circular structure is shown in Fig 3.7.

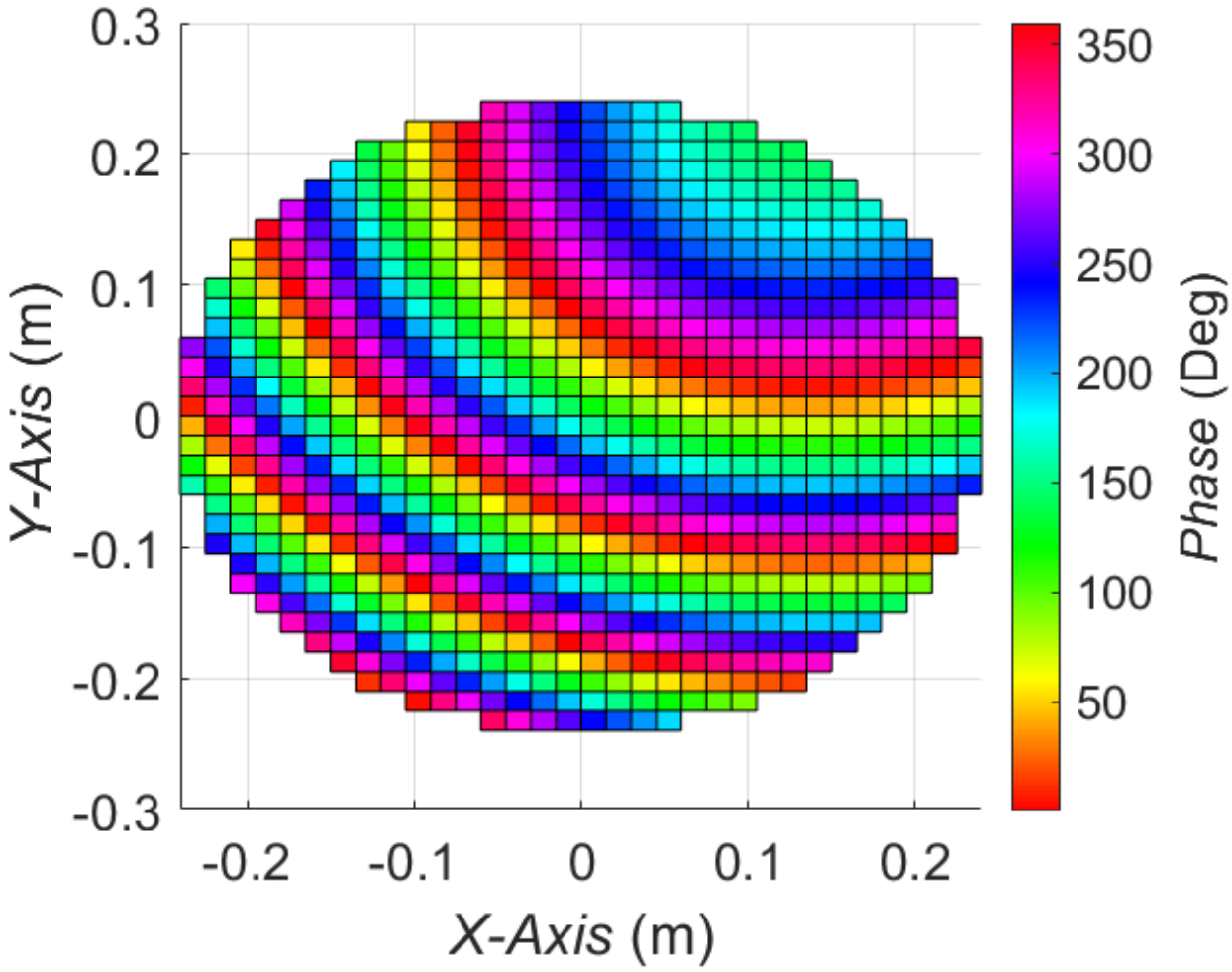

Figure 3.7: Phase distribution calculated by theoretical analysis.

The phase distribution on the reflecting surface realizes beam steering in any direction. Therefore one of the most important parts in reflectarray design is reflection phase shift of each unit cell from 0 to 2π. The different phase tuning techniques are discussed in the previous section. In this thesis, the varactor-controlled phase shift method for reconfigurable beam steering is presented.

3.2.2 Feed Antenna Position

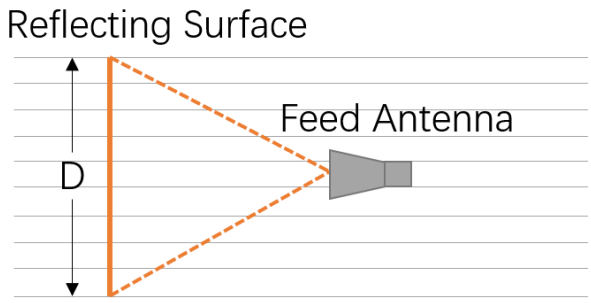

Figure 3.8: Side view of reflectarray system and feed position.

In the reflectarray system, the position of feed antenna is important to the performance of antenna. In general, the feed antenna is located on the top of the center of the reflecting surface which is also called center-fed symmetric reflectarray as shown in Fig 3.8. This kind of antenna position is easy to set and calculate, however, the feed blockage is a physical characteristic that exists in reflectarray, where the feed antenna blocks some of the radiation. This effect, called aperture blockage, causes a reduction in antenna gain and an increase in side lobe level. Aperture blockage is a function of the ratio of the blockage ratio to the reflectarray diameter as shown in Fig 3.9, which is known as blockage ratio. A_b is the blockage area projected onto the physical aperture of area A_p. In the next section, the aperture blockage is considered into aperture efficiency.

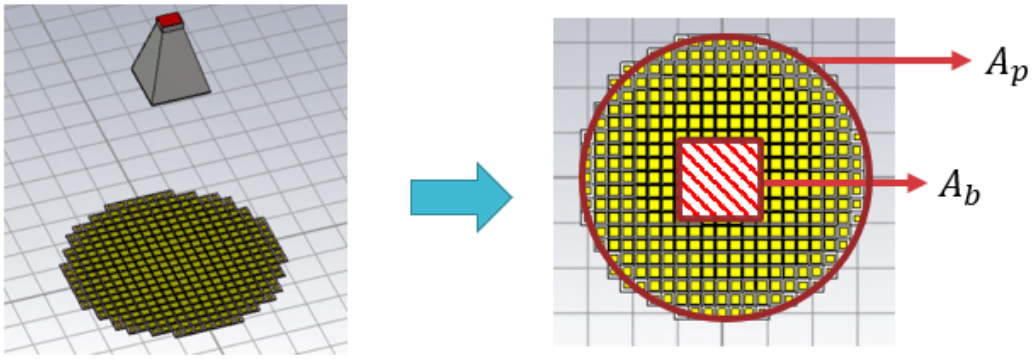

Figure 3.9: Feed blockage.

Chapter 4

Directivity and Efficiency of the Reflectarray

The reflectarray antenna design begins with a specific gain requirement. The gain of a reflectarray antenna is based on the antenna directivity and radiation efficiency. In the thesis, the directivity of the reflecting surface is analyzed based on the calculation of aperture efficiency. The directivity of a reflectarray antenna is proportional to the electrical size of the reflecting surface similar to apertures of traditional reflector antennas. The effective directivity is calculated as the product of the aperture efficiency and maximum aperture directivity. Through the aperture efficiency analysis, the required sizes of the reflectarray antenna and reflecting surface can be estimated to achieve the desired directivity and gain. The basic consideration of the aperture efficiency in a reflectarray are spillover efficiency and taper efficiency. In the thesis, these two aperture efficiency and achievement efficiency are analyzed to obtain a feed position for the highest reflectarray directivity. Other aperture efficiency including the efficiency factors associated with the feed loss, reflectarray element loss, polarization loss, and mismatch loss also have effects on the directivity of reflectarray.

4.1 Directivity and Gain of Aperture Antenna

One definition of the antenna directivity is given by [47, p. 52]

$$D = \frac{4\pi U_m}{P} \tag{4.1}$$

where U_m is the maximum of the radiation intensity and P is the total radiated power evaluated by integrating over all radiation space. For an aperture antenna, in the case of main beam peak which is broadside, the maximum of the radiation intensity U_m and radiated power can be determined by [47, p. 361]

$$U_m = \frac{\beta^2}{8\pi^2\eta}\left|\iint_{S_a} \vec{E_a} ds'\right|^2 \tag{4.2}$$

$$P = \frac{1}{2\eta}\iint_{S_a} \left|\vec{E_a}\right|^2 ds' \tag{4.3}$$

where β is propagation constant, η is wave impedance and $\vec{E_a}$ is aperture field. By substituting (4.2) and (4.3) in (4.1), one gives a simplified equation of directivity for aperture antenna [47, p. 362]

$$D = \frac{4\pi}{\lambda^2}\frac{\left|\iint_{S_a} \vec{E_a} ds'\right|^2}{\iint_{S_a} \left|\vec{E_a}\right|^2 ds'} \tag{4.4}$$

This formula assumes that the pattern peak is directed to broadside of the aperture. If the aperture distribution is of uniform amplitude and phase distribution, then (4.4) reduces to [47, p. 362]

$$D_u = \frac{4\pi}{\lambda^2} A_p \tag{4.5}$$

where A_p is the physical aperture area. Note that this is a general result based on a uniform amplitude and phase aperture.

Gain of antenna equals directivity reduced by the amount of power lost on the antenna structure. From the definition of radiation efficiency and gain, the relationship between gain and directivity is given by [47, p. 363]

$$P = e_r P_{in} \tag{4.6}$$

$$G = \frac{4\pi U_m}{P_{in}} \tag{4.7}$$

$$G = \frac{4\pi}{\lambda^2} A_e = \frac{4\pi}{\lambda^2} \eta_{ap} A_p = \eta_{ap} D_u = e_r D \tag{4.8}$$

where P_{in} is input power, A_e is the effective aperture area, e_r is radiation efficiency and aperture efficiency η_{ap} is to measure how efficiently the antenna physical area is utilized.

4.2 Aperture Efficiency Analysis

The total aperture efficiency can be separated into several parts for general use [47, p. 364].

$$\eta_{ap} = e_r \eta_s \eta_t \eta_a \tag{4.9}$$

where η_s is spillover efficiency, η_t is taper efficiency and η_a is achievement efficiency. These different efficiencies are discussed in the following.

In most aperture antennas, radiation losses are very low that $e_r \approx 1$ and $G \approx D$. To analyze the directivity and gain of the reflectarray, the calculation of aperture efficiency is discussed.

4.2.1 Feed Antenna Model

In the thesis, the cos^q pattern [48] is used to represent radiation of a feed antenna. The reflectarray system is shown as Fig 4.1. Center point C is the feed beam point that the radiation wave of feed antenna directed at this point. θ_0 is the angle between wave incident on feed beam point and wave to the rim of the surface which is subtended angle.

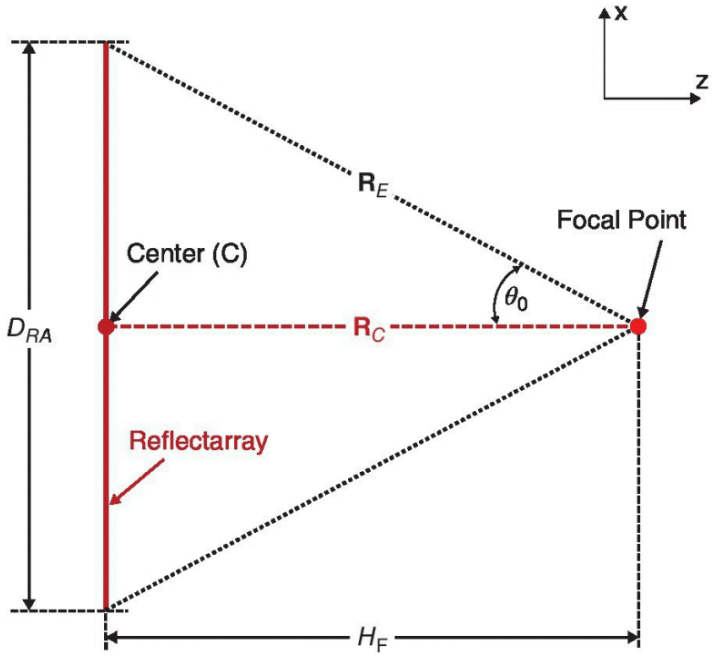

Figure 4.1: Side view of center-fed reflectarray system.

The radiation pattern of feed antenna is defined as [47, p. 412]

$$F_f(\theta_f) = \begin{cases} \cos^q\theta_f & (0 \leq \theta_f \leq \pi/2). \\ 0 & elsewhere \end{cases} \tag{4.10}$$

θ_f is a variable of subtended angle which is normalized to a peak of unity at $\theta_f = \theta_0$.

This radiation model of feed antenna represents the directivity and shape of the pattern by a single parameter q. Although this kind of model is idealistic, these patterns have

advantages that a closed form solutions can be obtained. Also they are used to represent the main lobe of many practical antennas.

Here, the expression for the gain of the feed antenna is given by [47, p. 412]

$$G_f = \frac{4\pi}{\int_0^{2\pi}\int_0^{\pi} |F_f(\theta_f, \phi')|^2 \sin\theta_f d\theta_f d\phi'} \tag{4.11}$$

$F_f(\theta_f, \phi')$ is feed antenna pattern. Then using the radiation pattern model in (4.10), it becomes [47, p. 412]

$$G_f = 2(2q+1) \tag{4.12}$$

From the equation we can obtain a relationship between gain of the feed antenna and factor q. This model is used for an ideal feed antenna to calculate efficiency of the reflectarray system. Practical feed antenna can be different considering other factors like balance of E and H pattern.

4.2.2 Illumination and Achievement Efficiency

A. Spillover efficiency

Spillover efficiency is related to the feed antenna location and area of the reflecting surface. Spillover efficiency η_s is defined as the percentage of the radiated power from the feed antenna which is intercepted by the reflecting surface. Due to the finite size of the reflecting surface, some of the radiation from the feed antenna will travel away from the main axis at an angle greater than θ_0, thus not being reflected. This efficiency can be improved by moving the feed closer to the reflecting surface, or by increasing the size of the reflecting surface. From the definition of spillover efficiency, it can be evaluated by the

following equation [47, p. 411]

$$\eta_s = \frac{\int_0^{2\pi}\int_0^{\theta_0}\left|F_f(\theta_f,\phi')\right|^2\sin\theta_f d\theta_f d\phi'}{\int_0^{2\pi}\int_0^{\pi}\left|F_f(\theta_f,\phi')\right|^2\sin\theta_f d\theta_f d\phi'} \tag{4.13}$$

where the denominator is the total power radiated by the feed antenna and the numerator is the incident power that intercepted by the reflecting surface. Using the feed pattern of $cos^q(\theta)$ form, one can derive the following expression for the spillover efficiency [47, p. 412]

$$\eta_s = 1 - \cos^{2q+1}(\theta_0) \tag{4.14}$$

B. Taper efficiency

The aperture taper efficiency is due to the non-uniform amplitude distribution on the aperture plane. The taper efficiency depends on many factors in reflectarray system such as radiation pattern of the feed antenna, position of the feed antenna, shape of the reflecting surface and radiation pattern of each unit cell. In the thesis, the analytic method of the aperture taper calculation is introduced.

Aperture taper efficiency is obtained by working with that portion of the power that reaches the aperture. That is, if we ignore achievement and spillover losses, (4.4) for a circular aperture of radius a leads to [47, p. 410]

$$\eta_t = \frac{1}{\pi a^2}\frac{\left|\int_0^{2\pi}\int_0^{a} E_a(\rho',\phi')\rho' d\rho' d\phi'\right|^2}{\int_0^{2\pi}\int_0^{a}\left|E_a(\rho',\phi')\right|^2\rho' d\rho' d\phi'} \tag{4.15}$$

where $E_a(\rho',\phi')$ is the aperture magnitude distribution.

Aperture taper efficiency measures the uniformity of the magnitude distribution of the feed pattern over the surface of the reflectarray. The phase component of aperture field is

included in phase error efficiency which is a part of achievement efficiency. The expression can be written directly in terms of the known feed antenna pattern by transforming to feed angles [47, p. 411]

$$\eta_t = \frac{4F^2}{\pi a^2} \frac{\left| \int_0^{2\pi} \int_0^{\theta_0} F_f(\theta_f, \phi') \tan\frac{\theta_f}{2} d\theta_f d\phi' \right|^2}{\int_0^{2\pi} \int_0^{\theta_0} |F_f(\theta_f, \phi')|^2 \sin\theta_f d\theta_f d\phi'} \tag{4.16}$$

The evaluation of taper efficiency is complicated. The effect including spillover and taper efficiency can be called as illumination efficiency. Some equations of illumination efficiency with different q factor are given by [47, p. 412]

$$\eta_i = \cot^2\frac{\theta_0}{2} \begin{cases} 24[\sin^2\frac{\theta_0}{2} + ln(cos\frac{\theta_0}{2})]^2 & q = 1 \\ 40[\sin^4\frac{\theta_0}{2} + ln(cos\frac{\theta_0}{2})]^2 & q = 2 \\ 14[\frac{1}{2}\sin^2\theta_0 + \frac{1}{3}(1-\cos\theta_0)^3 + 2ln(\cos\frac{\theta_0}{2})]^2 & q = 3 \end{cases} \tag{4.17}$$

The total efficiency analysis mainly focuses on the spillover efficiency and aperture taper efficiency. To further analyze the effect of reflectarray system to the efficiency, the factors including subtended angle and feed antenna pattern are estimated. We assume that the phase distribution is uniform, when q equal to 6, the relationship of subtended angle and efficiency based on (4.14) and (4.16) is shown in Fig 4.2. With the subtended angle increasing, the spillover efficiency increasing while the taper efficiency decreasing.

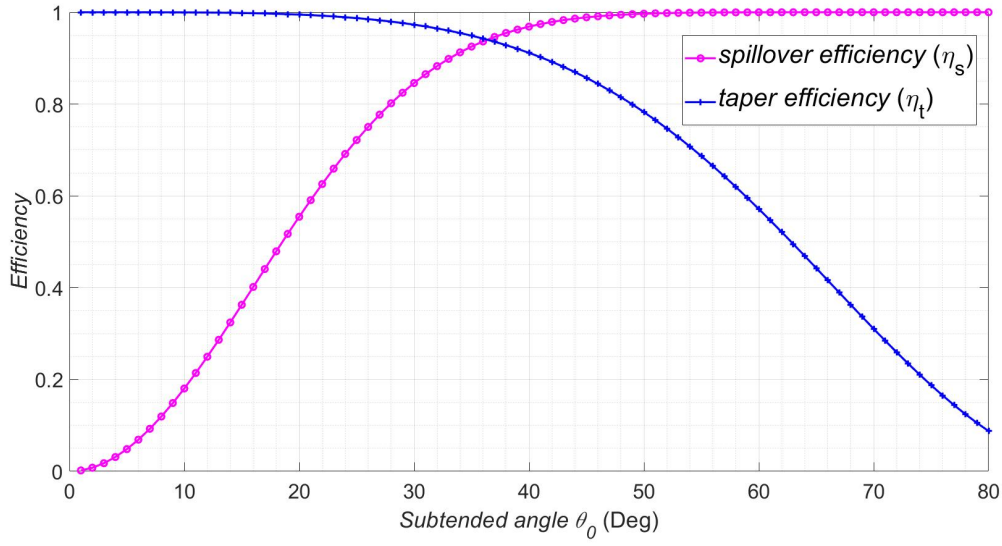

Figure 4.2: Efficiency versus subtended angle ($q = 6$).

The feed antenna radiation pattern is another important effect on efficiency. The radiation $\cos^q(\theta)$ model uses factor q to represent radiation pattern. The relationship of factor q and illumination efficiency including the spillover efficiency and tape efficiency is given in Fig 4.3.

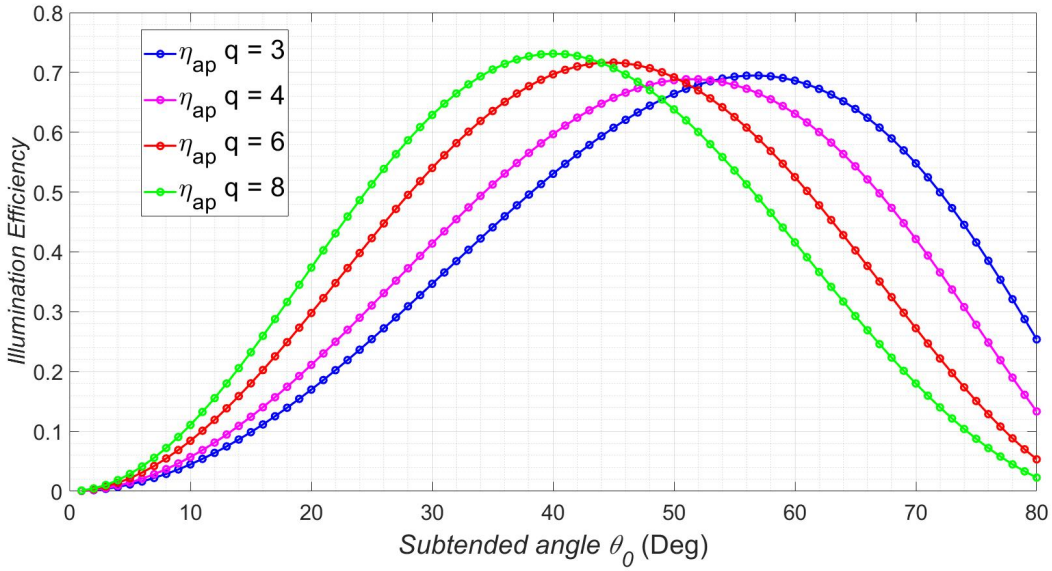

Figure 4.3: Illumination efficiency versus factor q.

C. Achievement efficiency

Besides spillover efficiency and aperture taper efficiency, several factors that reduce gain for practical implementation reasons are lumped together can be called as achievement efficiency. The achievement efficiency is expressed using subefficiencies as [47, p. 413]

$$\eta_a = \eta_{rs}\eta_{cr}\eta_b\eta_\phi \tag{4.18}$$

where η_{rs} is random surface error efficiency which is associated with the gain loss from random surface errors, η_{cr} is cross-polarization efficiency because feed antennas have a component that is orthogonal to the desired polarization, η_b is the blockage efficiency that measures how much radiation is blocked by the feed antenna, and η_ϕ is phase error efficiency that represents nonuniform phase across the aperture and phase error due to feed antenna leading to gain loss and pattern deterioration. These efficiencies also cause gain losses, but are usually small compared to spillover and taper loss.

Blockage efficiency is analyzed in this thesis. In the case of the center-fed symmetric reflectarray antenna, the feed antenna is located at the top of surface center which may block some radiation of surface and hence degrades the performance by reducing the gain and also increasing cross-polarization. A simple approximate formula is available for the aperture blockage efficiency [47, p. 414]

$$\eta_b = [1 - \frac{1}{\eta_t}\frac{A_b}{A_p}]^2 \tag{4.19}$$

where A_b is the blockage area projected onto the physical aperture of area A_p.

Feed blockage is inevitable in the case of the centre-fed reflectarray system. The larger the feed assembly is, the lower is the blockage efficiency. However, a center-fed reflectarray can be designed to avoid the blockage completely by setting the direction of the outgoing

beam appropriately.

From the analysis of effects on the reflectarray efficiency, the reflectarray system's setting can be optimized to obtain a higher directivity.

Chapter 5

Full Wave Simulation Result

The reflectarray system introduced in this thesis consists of a feed antenna and a reflecting surface. The microstrip patch antenna introduced in the previous chapter is using as the feed antenna. The reflecting surface composes of array of dog-bone shaped unit cells with varactors inserted. In this section, the configuration of the reflectarray system is given and far-field result of the reflecting radiation is plotted with the beam direction changing under the control of varactors, that is the reconfigurable reflectarray antenna.

The center-fed symmetrical reflectarray is given in full-wave simulation software (CST) to analyze the antenna performance. The reflecting surface is selected to be circular for comparison to the result of mathematical calculation.

5.1 Reflectarray System Setting

The dog-bone shaped structure is used as the unit cell of the reflecting surface as shown in Fig 5.1. The unit cell is simulated in full-wave simulation software with the specific unit cell boundary condition. Series RLC lumped elements are used in full-wave simulation

software to represent the effect of the varactors. Based on the analysis of the phase shift on the surface of unit cell, the capacitance of the varactors is given specifically for each unit cell related to Table 2.2.

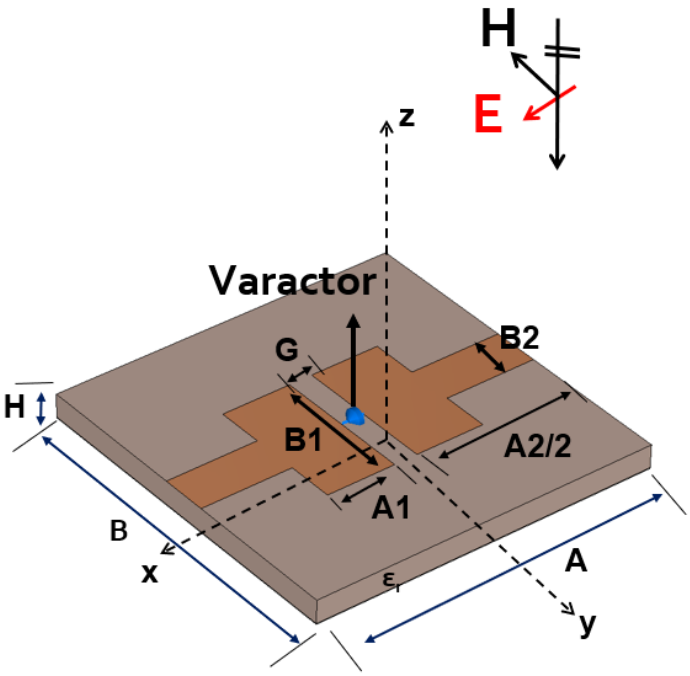

Figure 5.1: Dog-bone unit cell element with varactor.

The unit cell structure was introduced specifically in the previous chapter. All the parameters are list in Table 5.1.

Table 5.1: Dog-bone structure parameters

Para.	Value(mm)	Para.	Value(mm)
A	15	A2	14
B	15	B2	2
A1	3	G	1
B1	6	H	1

The microstrip patch antenna introduced in the previous chapter is used as the feed

antenna.

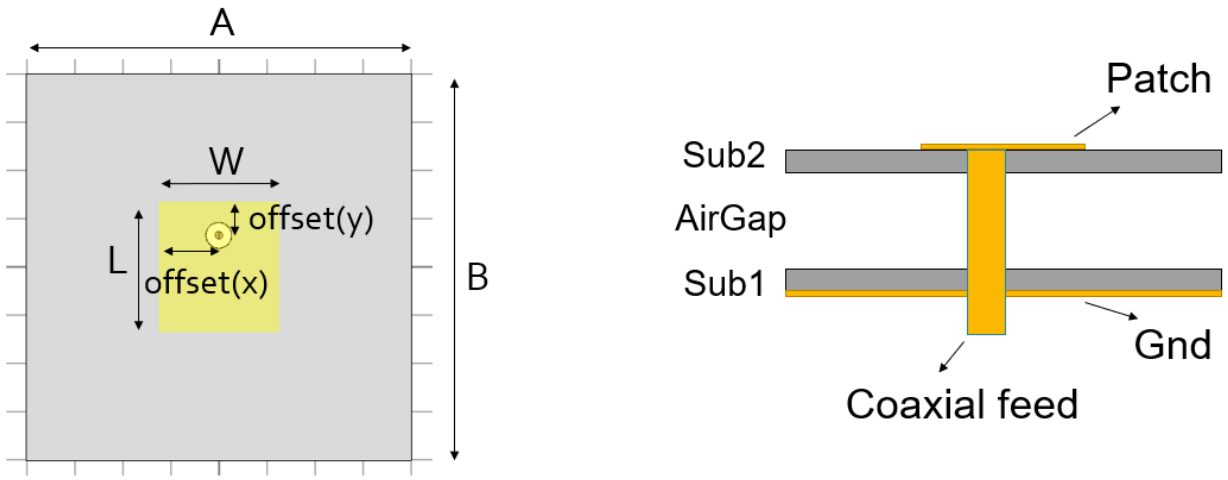

Figure 5.2: Top and side view of feed antenna.

All the parameters of feed antenna are list in Table 5.2.

Table 5.2: Feed antenna structure parameters

Para.	Value(mm)	Para.	Value(mm)	Para.	Value(mm)
A	80	W	25	offset(x)	12.5
B	80	L	27	offset(y)	7
Hsub1	0.28	Hsub2	0.28	H_AirGap	3.5

The diameter of circular reflecting surface is 500 mm. The feed antenna is located above the surface center. The top view of the reflectarray system is shown in Fig 5.3. The subtended angle is one of the factors that affect the gain performance of the reflectarray system. In this case, the subtended angle is set as 45° so that the height of the feed antenna can be calculated and is given by 250 mm.

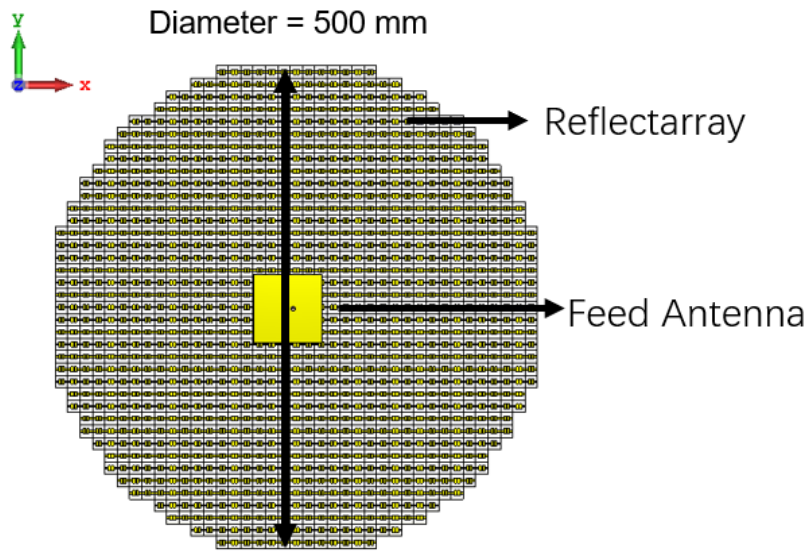

Figure 5.3: Top view of circular reflecting surface.

The whole reflectarray system setting in full-wave simulation software is shown in Fig 5.4. For varactors in the each unit cell, specific values of the resistance, inductance and capacitance are given to obtain a reasonable phase distribution at 4.4 GHz.

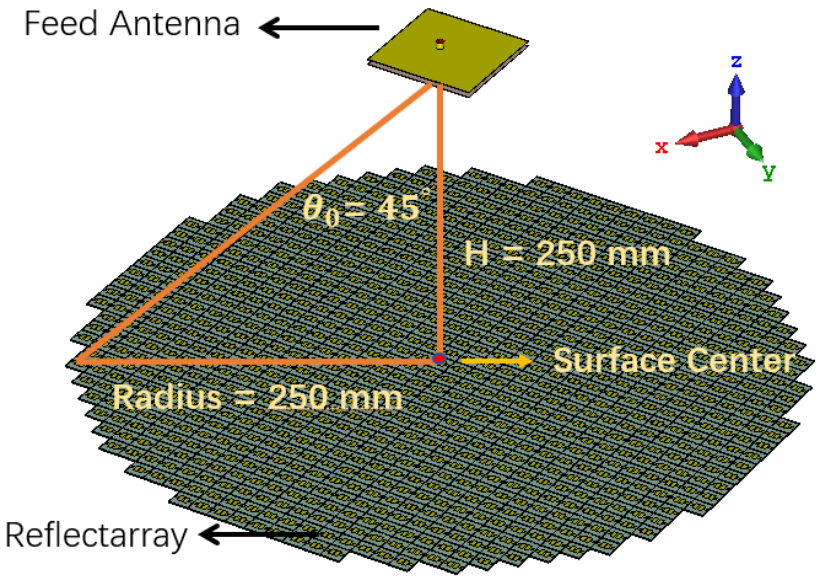

Figure 5.4: Reflectarray Geometry.

5.2 Beam Steering Result

To realize reconfigurable reflecting surface and beam steering for reflectarray system, the varactors provide linear control of phase shift across the surface. In the thesis, three different radiation beam directions are shown. (θ_r, ϕ_r) is the maximum direction of the radiation pattern in the far-field.

Case A. Radiation beam direction: $(\theta_r = 45°, \phi_r = 45°)$

To get a specific phase distribution on the reflecting surface, the bias voltage for each varactor in the unit cell is controlled accordingly. The phase distribution is calculated in Matlab and related bias voltage distribution based on Fig 2.12 is shown in Fig 5.5.

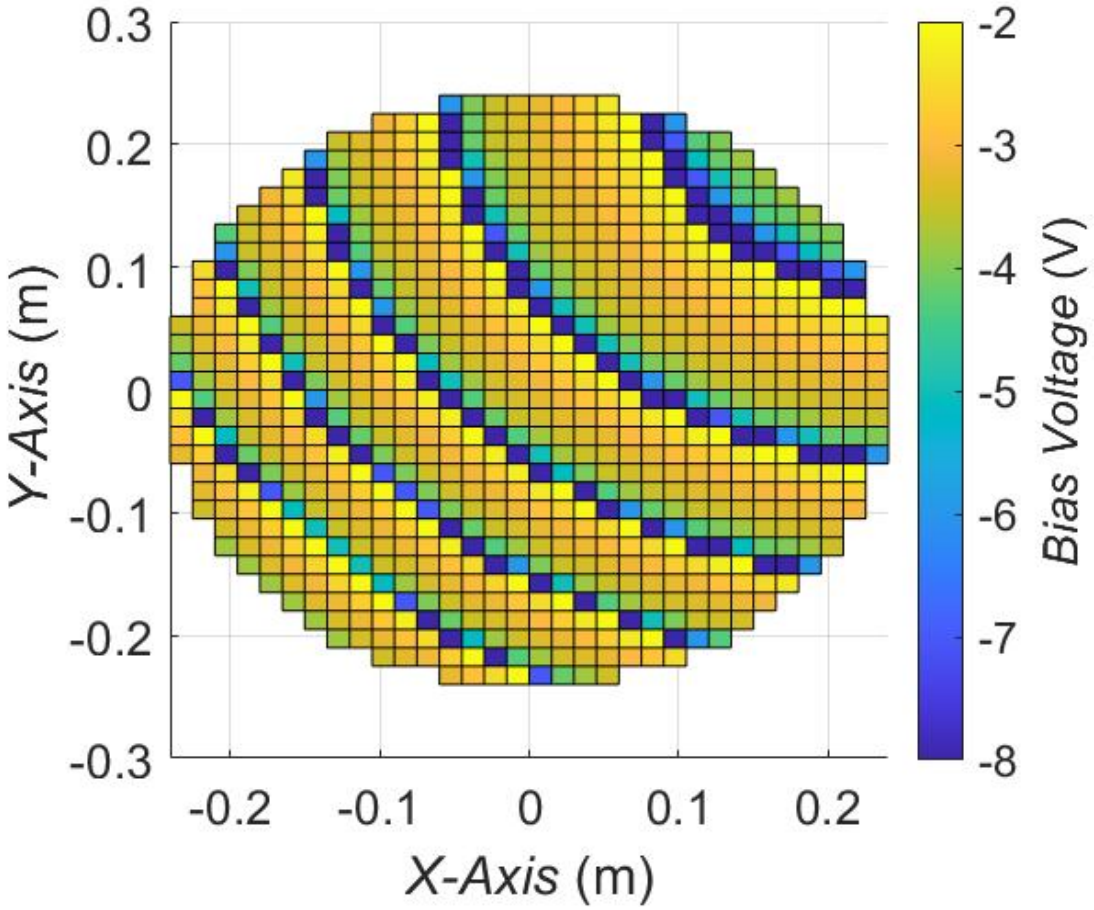

Figure 5.5: Bias voltage distribution at $(\theta_r = 45°, \phi_r = 45°)$.

The 3D far-field radiation pattern in the full-wave simulation result is shown in Fig 5.6. Note the pencil-shaped beam, synthesized by the reflectarray, is steered at $(\theta_r = 45°, \phi_r = 45°)$.

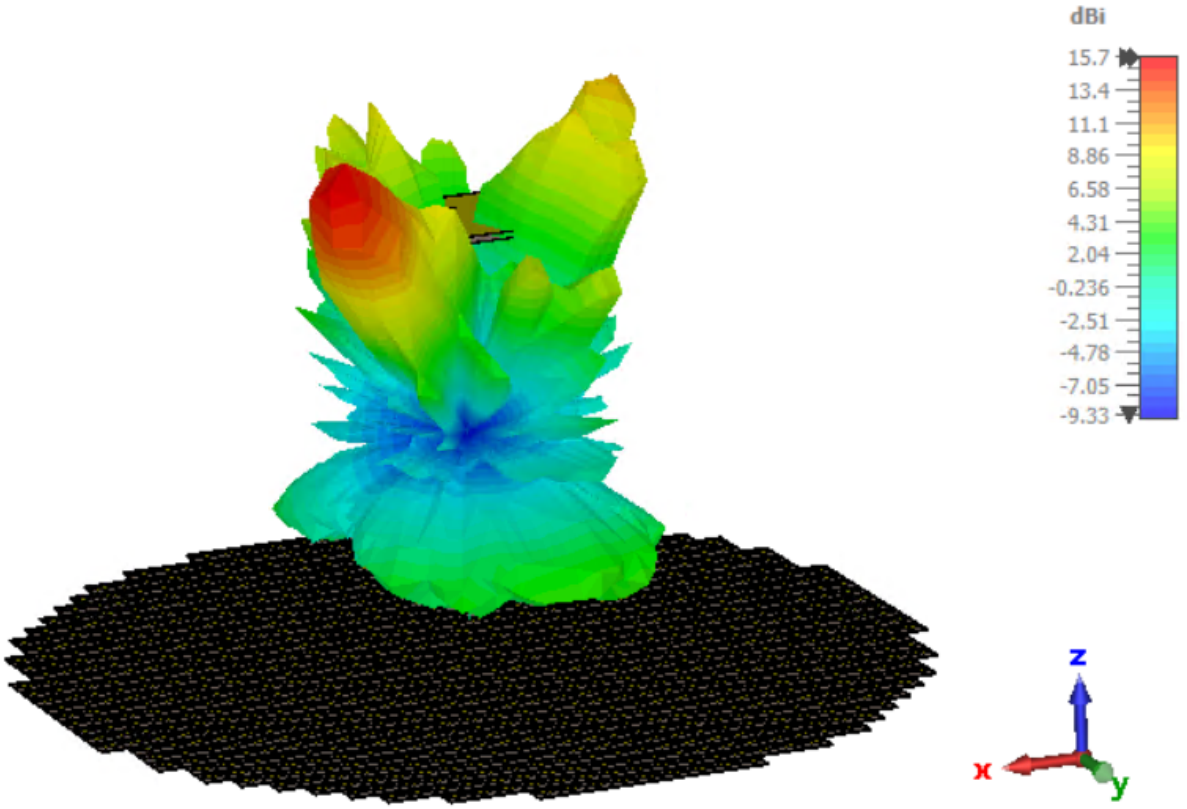

Figure 5.6: 3D far-field radiation pattern at $(\theta_r = 45°, \phi_r = 45°)$.

To identify the reflecting beam direction, the polar plots of the far-field radiation are given in the case of $\theta_r = 45°$ and $\phi_r = 45°$. As shown in Fig 5.7 and Fig 5.8, the reflected beam is steered to $(\theta_r = 45°, \phi_r = 45°)$ in spherical coordinates which agrees with the requirement in the reflectarray system setting.

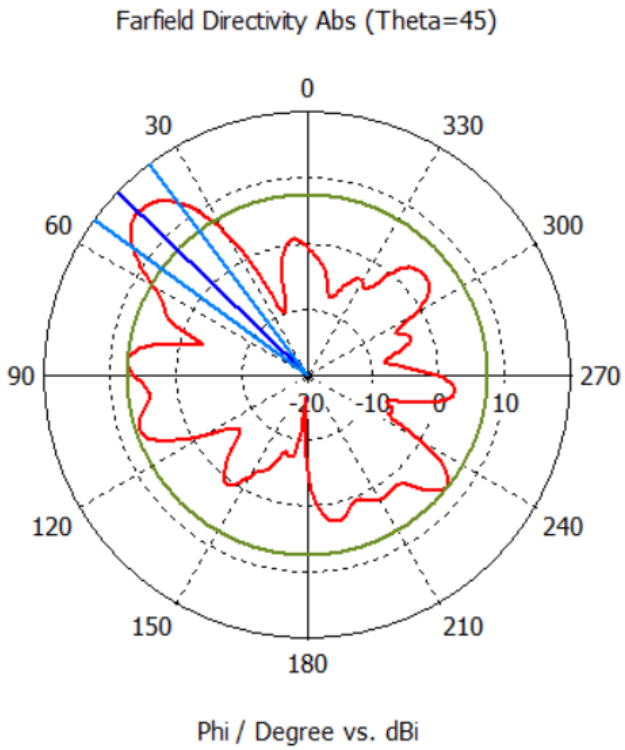

Figure 5.7: Radiation pattern in polar plot when ($\theta_r = 45°$).

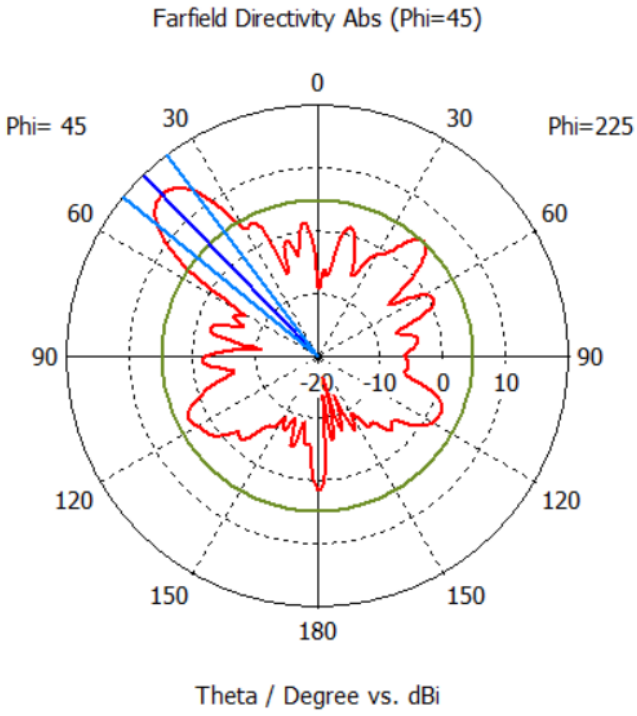

Figure 5.8: Radiation pattern in polar plot when ($\phi_r = 45°$).

Case B. Radiation beam direction: $(\theta_r = 20°, \phi_r = 20°)$

Similar to the settings in case A, we set a different bias voltage value for each unit cell element to obtain a specific phase distribution on the reflecting surface. The bias voltage distribution of the circular reflecting surface is shown in Fig 5.9.

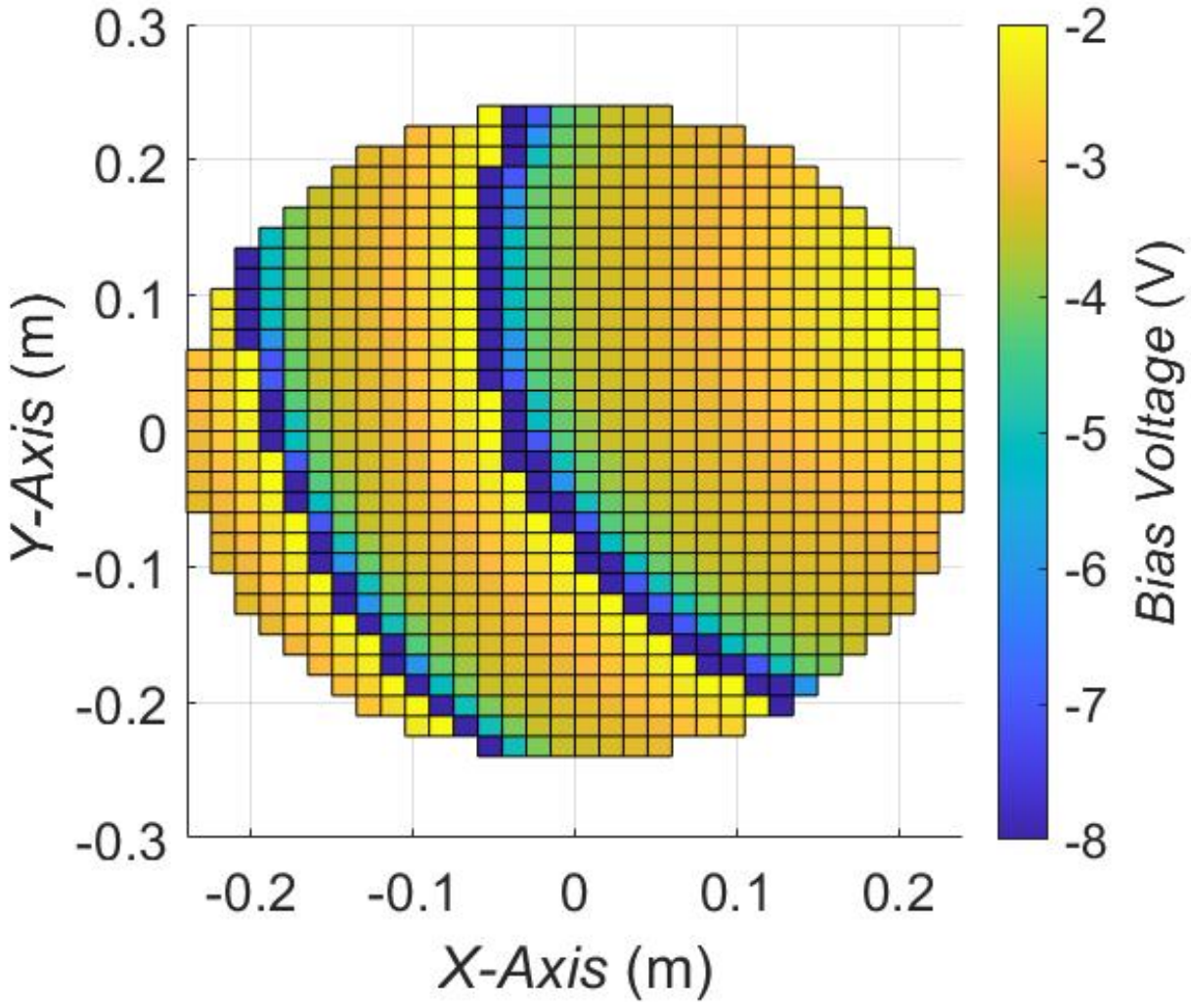

Figure 5.9: Bias voltage distribution at $(\theta_r = 20°, \phi_r = 20°)$.

The 3D far-field radiation pattern in the full-wave simulation result is shown in in Fig 5.10. The main beam is steered at $(\theta_r = 20°, \phi_r = 20°)$.

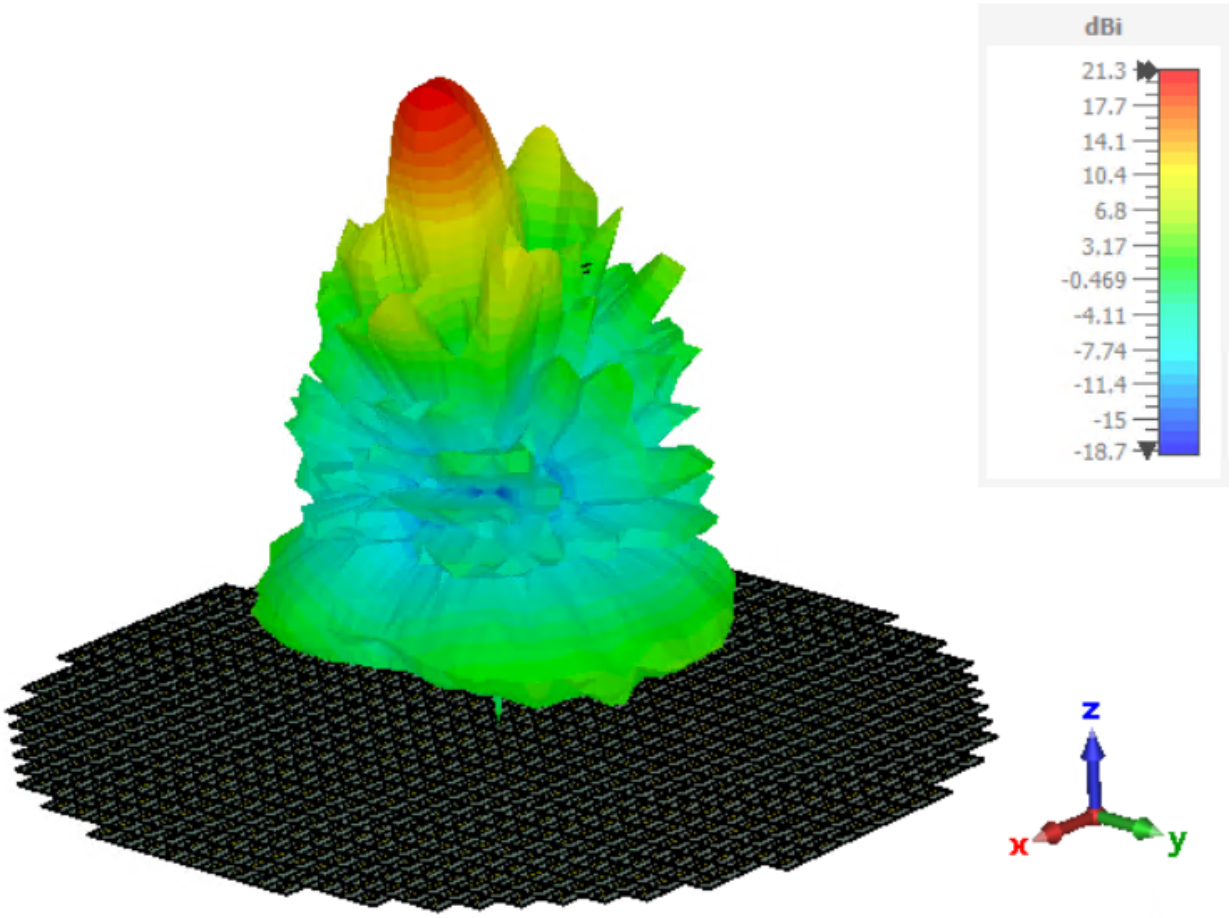

Figure 5.10: 3D far-field radiation pattern at $(\theta_r = 20°, \phi_r = 20°)$.

To identify the reflecting beam direction, the polar plots of the far-field radiation are given in the case of $\theta_r = 20°$ and $\phi_r = 20°$. As shown in Fig 5.11 and Fig 5.12, the reflecting beam is directed to $(\theta_r = 20°, \phi_r = 20°)$ in spherical coordinates which agrees with the requirement in the reflectarray system setting.

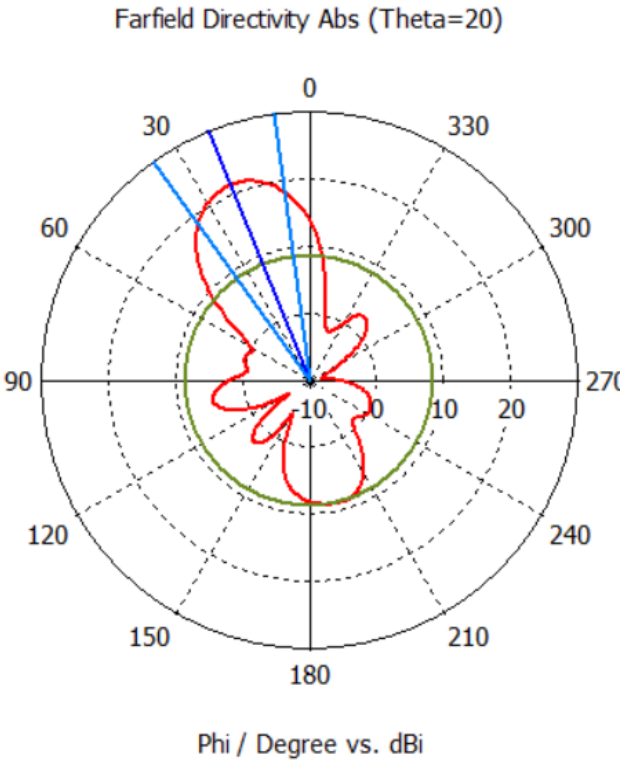

Figure 5.11: Radiation pattern in polar plot when ($\theta_r = 20°$).

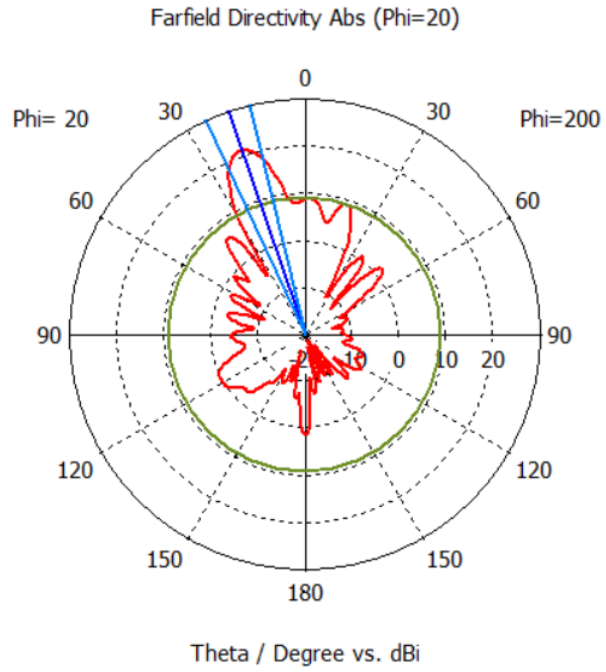

Figure 5.12: Radiation pattern in polar plot when ($\phi_r = 20°$).

Case C. Radiation beam direction: $(\theta_r = 0°, \phi_r = 0°)$ (broadside)

Here, we have the final case that beam direction is the broadside. The bias voltage distribution of the circular reflecting surface is shown in Fig 5.13.

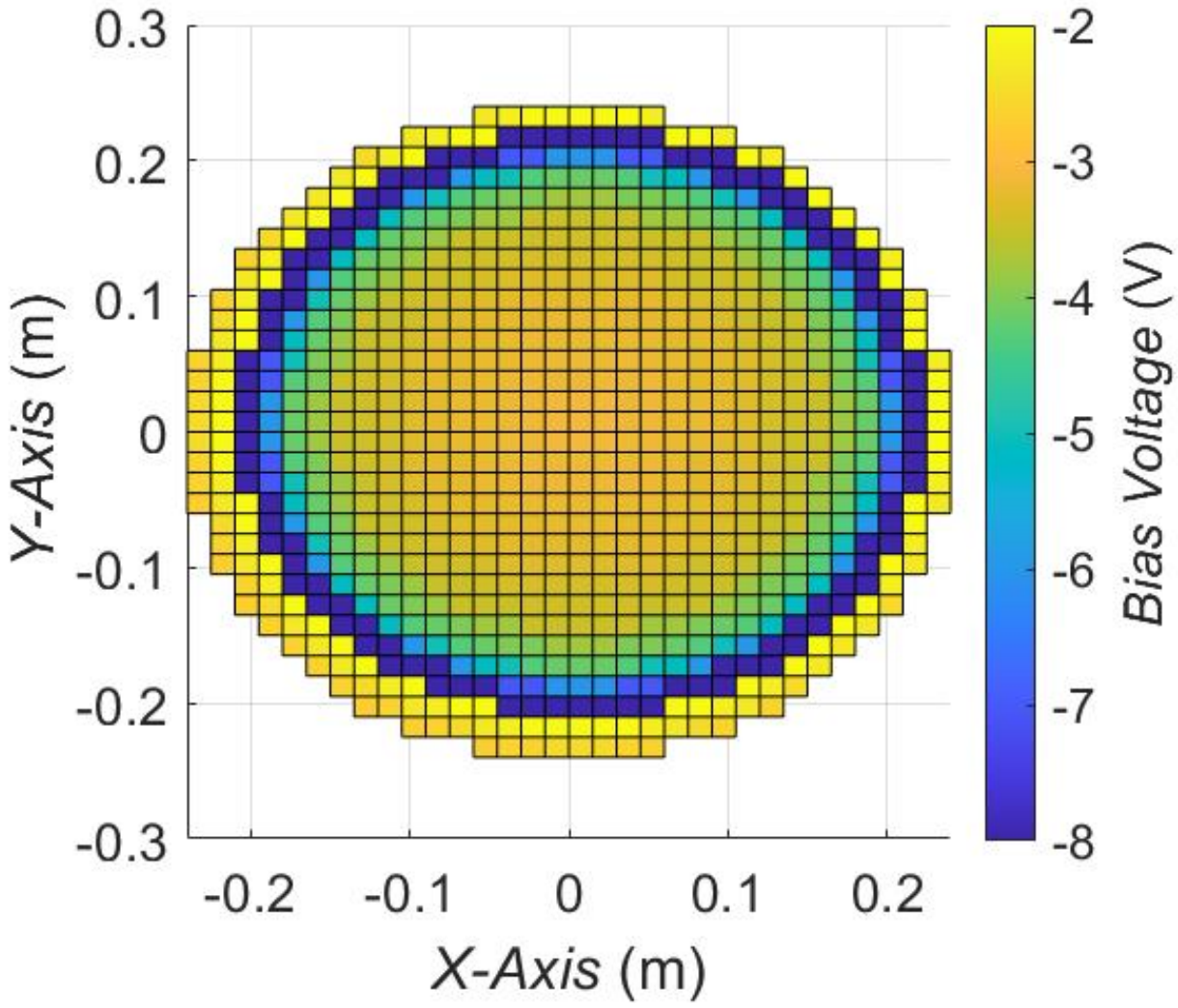

Figure 5.13: Bias voltage distribution at $(\theta_r = 0°, \phi_r = 0°)$.

The 3D far-field radiation pattern in the full-wave simulation result is shown in Fig 5.14. The main beam is steered at broadside ($\theta_r = 0°, \phi_r = 0°$).

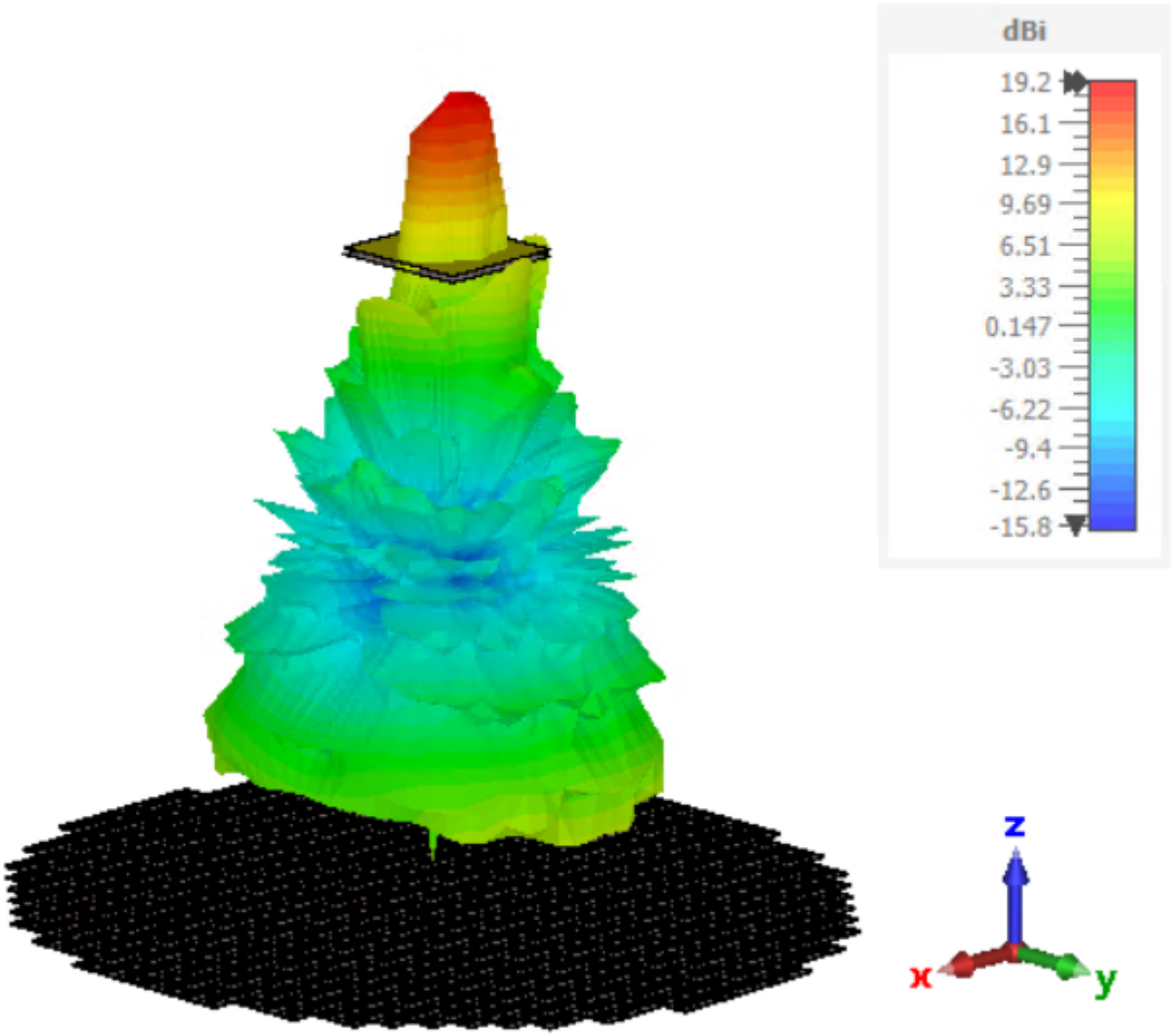

Figure 5.14: 3D far-field radiation pattern at ($\theta_r = 0°, \phi_r = 0°$).

To identity the reflecting beam direction, the polar plots of the far-field radiation are given in the case of $\theta_r = 0°$ and $\phi_r = 0°$. As shown in Fig 5.15 and Fig 5.16, the reflecting beam is directed to ($\theta_r = 0°, \phi_r = 0°$) which is broadside in spherical coordinates which agrees with the requirement in the reflectarray system setting.

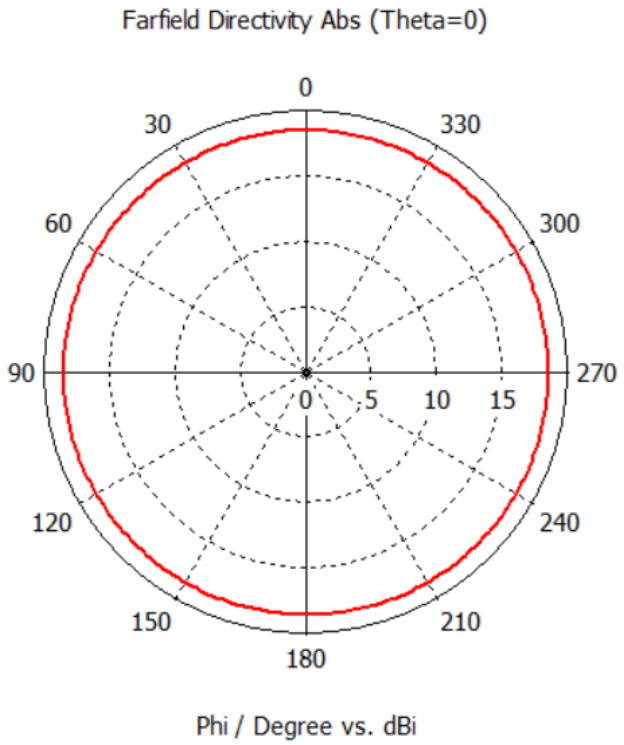

Figure 5.15: Radiation pattern in polar plot when ($\theta_r = 0°$).

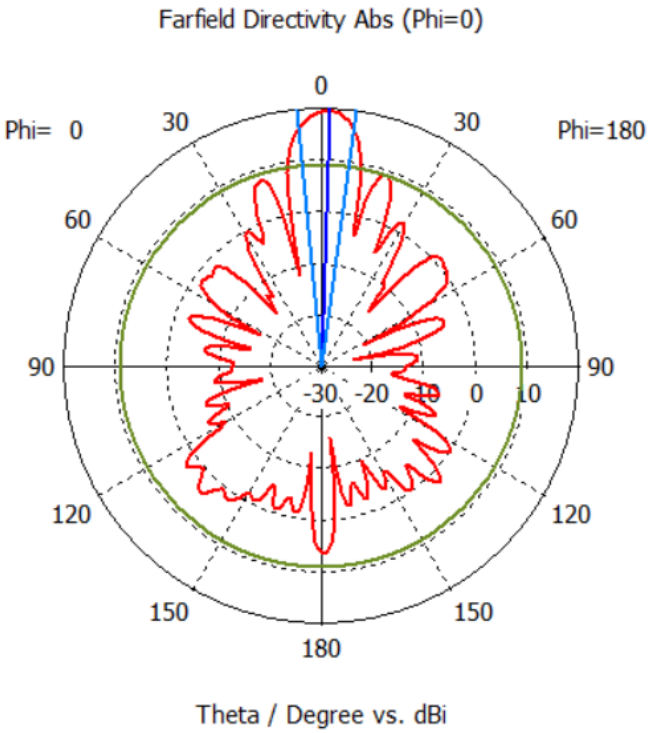

Figure 5.16: Radiation pattern in polar plot when ($\phi_r = 0°$).

The far-field radiation result shows that three different radiation beam directions are realized which means that the radiation beam direction can be adjusted by varactors control. The far-field results of three cases show that a pencil-shaped beam is produced by reflecting surface while the side lobe level is increasing because of feed antenna blockage. This kind of reconfigurable reflectarray antenna can perform beam steering in upper-hemisphere of the coordination.

The directivity of the reflecting surface is obtained in the full-wave simulation and compared to the result from mathematical method in Matlab.

The directivity is calculated based on (4.8) and (4.9) that

$$D = \frac{4\pi}{\lambda^2}\eta_s\eta_t\eta_b A_p \tag{5.1}$$

which includes the spillover, taper and blockage efficiency. In the case of broadside direction. The result that directivity varies with subtended angle calculated in Matlab is shown in Fig 5.17.

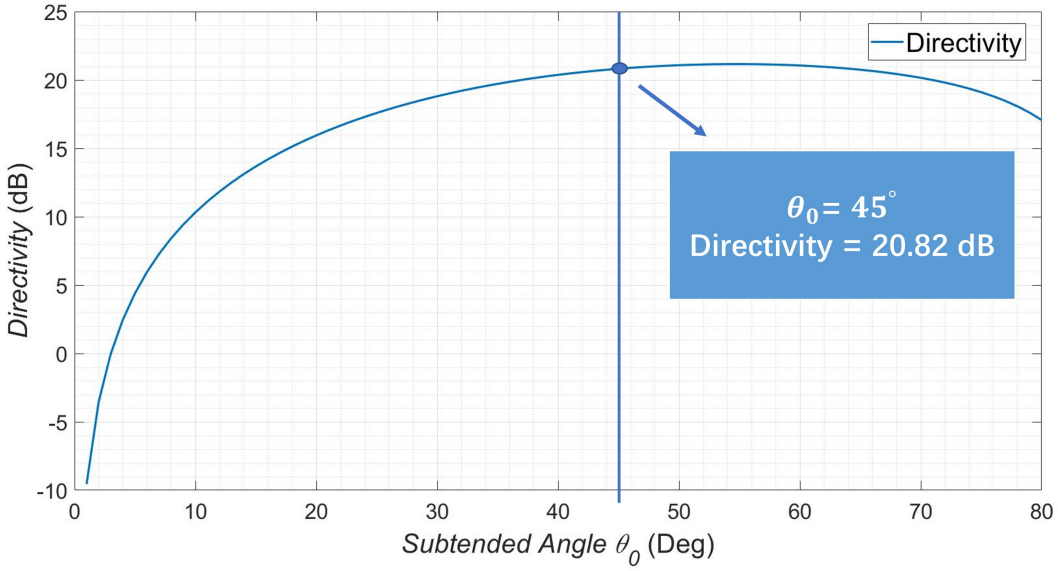

Figure 5.17: Calculated directivity versus subtended angle

The directivity of the reflecting surface from mathematical analysis varies with the subtended angle increasing. For the special case that subtended angle $\theta_0 = 45°$, the directivity result is 20.82 dB.

The full-wave simulation directivity result is shown in Fig 5.18. In the case of the reflecting beam direct to broadside, the directivity result is 19.2 dB.

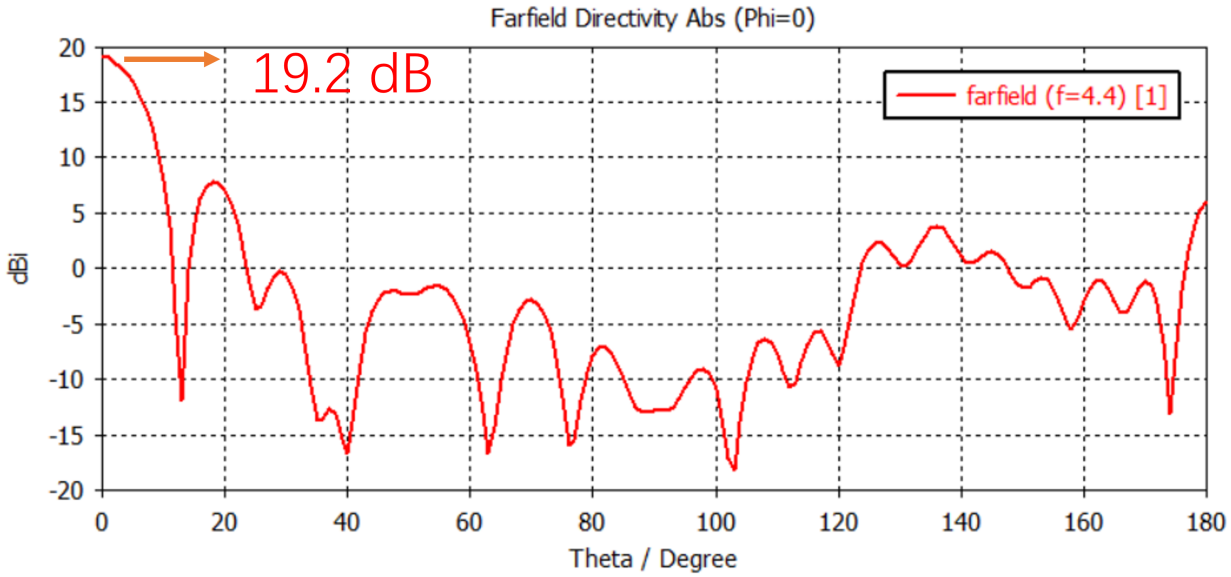

Figure 5.18: One dimensional result of radiation pattern for broadside case.

The result ofthe full-wave simulation has 1.5 dB deviation from that from mathematical calculation. Other losses except the spillover and taper are considered. Therefore, these two kinds of gain results agree with each other.

Chapter 6

Conclusion

A reconfigurable reflectarray antenna system has been proposed where three different reflecting beam directions are realized.

First the different unit cell elements are introduced to make up the metasurface which is used as the reflecting surface of the reflectarray system. To control the phase distribution on the unit cell element surface, varactors diodes are inserted into the unit cell elements and then phase of reflection coefficient shift as the capacitance of varactors varying. Varactors parameters from manufacture's datasheet are transformed into series RLC circuits which can be used in full-wave simulation software (CST).

The reflectarray system consists of a feed antenna and a reflecting surface. The feed antenna uses a microstrip antenna with air gap inside the substrates to obtain higher gain. As a result, a patch antenna with gain of 9.64 dB is designed at 4.4 GHz and and is placed a certain distance above the center of the reflecting surface (center-fed configuration). To realize the specific radiation beam direction, the phase distribution on the reflecting surface has to be realized and programmed accordingly in each unit cell.

Directivity and gain analysis of reflectarray are based on the aperture efficiency calculations. The spillover efficiency and taper efficiency have major effect on the antenna directivity. The relationship between the aperture efficiency and the feed antenna pattern is analyzed. Also, how the total efficiency of the reflectarray system varies with the increasing subtended angle is shown.

The design of the reflectarray antenna system is based initially on the theoretical techniques which are later verified through full-wave simulations. This kind of reconfigurable reflectarray antenna can be used in 5G wireless communication for satisfying the requirement of beam steering in mobile communication system. In practice, a biasing mechanism has to be integrated in each unit cell in order to vary the capacitance and hence the phase. In the future, elements could be scaled or redesigned to obtain higher resonant frequencies and low loss varactors can be introduced to reduce the total losses in the reflecting surface.

Bibliography

[1] Efstratios Doumanis, G Goussetis, R Dickie, R Cahill, P Baine, M Bain, V Fusco, JA Encinar, and G Toso. Electronically reconfigurable liquid crystal based mm-wave polarization converter. *IEEE Transactions on Antennas and Propagation*, 62(4):2302–2307, 2014.

[2] Dowon Kim, Kitae Kim, Hogyeong Kim, Moonyoung Choi, and Jun-Hee Na. Design optimization of reconfigurable liquid crystal patch antenna. *Materials*, 14(4):932, 2021.

[3] Tayfun Nesimoglu and Cumali Sabah. A tunable metamaterial resonator using varactor diodes to facilitate the design of reconfigurable microwave circuits. *IEEE Transactions on Circuits and Systems II: Express Briefs*, 63(1):89–93, 2015.

[4] Cheng Huang, Changlei Zhang, Jianing Yang, Bo Sun, Bo Zhao, and Xiangang Luo. Reconfigurable metasurface for multifunctional control of electromagnetic waves. *Advanced Optical Materials*, 5(22):1700485, 2017.

[5] Dimitrios E Anagnostou, Guizhen Zheng, Michael T Chryssomallis, James C Lyke, George E Ponchak, John Papapolymerou, and Christos G Christodoulou. Design, fabrication, and measurements of an rf-mems-based self-similar reconfigurable antenna. *IEEE Transactions on Antennas and Propagation*, 54(2):422–432, 2006.

[6] Chang won Jung, Ming-jer Lee, GP Li, and Franco De Flaviis. Reconfigurable scan-beam single-arm spiral antenna integrated with rf-mems switches. *IEEE Transactions on antennas and propagation*, 54(2):455–463, 2006.

[7] Randy L Haupt and Michael Lanagan. Reconfigurable antennas. *IEEE Antennas and Propagation Magazine*, 55(1):49–61, 2013.

[8] Symeon Nikolaou, Ramanan Bairavasubramanian, Cesar Lugo, Ileana Carrasquillo, Dane C Thompson, George E Ponchak, John Papapolymerou, and Manos M Tentzeris. Pattern and frequency reconfigurable annular slot antenna using pin diodes. *IEEE Transactions on Antennas and Propagation*, 54(2):439–448, 2006.

[9] Nanli Mou, Shulin Sun, Hongxing Dong, Shaohua Dong, Qiong He, Lei Zhou, and Long Zhang. Hybridization-induced broadband terahertz wave absorption with graphene metasurfaces. *Optics express*, 26(9):11728–11736, 2018.

[10] Tong Cai, GuangMing Wang, ShiWei Tang, HeXiu Xu, JingWen Duan, HuiJie Guo, FuXin Guan, ShuLin Sun, Qiong He, and Lei Zhou. High-efficiency and full-space manipulation of electromagnetic wave fronts with metasurfaces. *Physical Review Applied*, 8(3):034033, 2017.

[11] Mooseok Jang, Yu Horie, Atsushi Shibukawa, Joshua Brake, Yan Liu, Seyedeh Mahsa Kamali, Amir Arbabi, Haowen Ruan, Andrei Faraon, and Changhuei Yang. Wavefront shaping with disorder-engineered metasurfaces. *Nature photonics*, 12(2):84–90, 2018.

[12] Yangbo Xie, Wenqi Wang, Huanyang Chen, Adam Konneker, Bogdan-Ioan Popa, and Steven A Cummer. Wavefront modulation and subwavelength diffractive acoustics with an acoustic metasurface. *Nature communications*, 5(1):1–5, 2014.

[13] Yuanmu Yang, Wenyi Wang, Parikshit Moitra, Ivan I Kravchenko, Dayrl P Briggs, and Jason Valentine. Dielectric meta-reflectarray for broadband linear polarization conversion and optical vortex generation. *Nano letters*, 14(3):1394–1399, 2014.

[14] HL Zhu, SW Cheung, Kwok Lun Chung, and Tong I Yuk. Linear-to-circular polarization conversion using metasurface. *IEEE transactions on antennas and propagation*, 61(9):4615–4623, 2013.

[15] Lei Chen, Qian Ma, Hong Bo Jing, Hao Yang Cui, Yi Liu, and Tie Jun Cui. Space-energy digital-coding metasurface based on an active amplifier. *Physical review applied*, 11(5):054051, 2019.

[16] Nate Lawrence, Jacob Trevino, and Luca Dal Negro. Aperiodic arrays of active nanopillars for radiation engineering. *Journal of Applied Physics*, 111(11):113101, 2012.

[17] Victor Georgievich Veselago. The electrodynamics of substances with simultaneously negative values of img align= absmiddle alt= eps/img and μ. *Physics-Uspekhi*, 10(4):509–514, 1968.

[18] Raj Mittra, Chi H Chan, and Tom Cwik. Techniques for analyzing frequency selective surfaces-a review. *Proceedings of the IEEE*, 76(12):1593–1615, 1988.

[19] Fan Yang and Yahya Rahmat-Samii. *Electromagnetic band gap structures in antenna engineering*. Cambridge university press Cambridge, UK, 2009.

[20] Peng Fei, Xin Wen, Peng Zhang, and Weihua Guo. A wideband single-layered circular polarizer with centrosymmetric dual-loop elements. In *2016 46th European Microwave Conference (EuMC)*, pages 1271–1274. IEEE, 2016.

[21] Alexandros P Feresidis, George Goussetis, Shenhong Wang, and John C Vardaxoglou. Artificial magnetic conductor surfaces and their application to low-profile high-gain planar antennas. *IEEE Transactions on Antennas and Propagation*, 53(1):209–215, 2005.

[22] Pedro J Castro, Joaquim J Barroso, and Joaquim P Leite Neto. Experimental study on split-ring resonators with different slit widths. 2013.

[23] Modeste Bodehou, Enrica Martini, Stefano Maci, Isabelle Huynen, and Christophe Craeye. Multibeam and beam scanning with modulated metasurfaces. *IEEE Transactions on Antennas and Propagation*, 68(3):1273–1281, 2019.

[24] Nir Shlezinger, Or Dicker, Yonina C Eldar, Insang Yoo, Mohammadreza F Imani, and David R Smith. Dynamic metasurface antennas for uplink massive mimo systems. *IEEE transactions on communications*, 67(10):6829–6843, 2019.

[25] Tie Jun Cui, Mei Qing Qi, Xiang Wan, Jie Zhao, and Qiang Cheng. Coding metamaterials, digital metamaterials and programmable metamaterials. *Light: science & applications*, 3(10):e218–e218, 2014.

[26] Tie Jun Cui, Shuo Liu, and Lei Zhang. Information metamaterials and metasurfaces. *Journal of materials chemistry C*, 5(15):3644–3668, 2017.

[27] Shuo Liu and Tie Jun Cui. Flexible controls of terahertz waves using coding and programmable metasurfaces. *IEEE journal of selected topics in quantum electronics*, 23(4):1–12, 2016.

[28] Raymond N Wilson. *Reflecting telescope optics II: manufacture, testing, alignment, Modern Techniques*. Springer Science & Business Media, 2013.

[29] D. Berry, R. Malech, and W. Kennedy. The reflectarray antenna. *IEEE Transactions on Antennas and Propagation*, 11(6):645–651, 1963.

[30] Keith Carver and James Mink. Microstrip antenna technology. *IEEE transactions on antennas and propagation*, 29(1):2–24, 1981.

[31] Payam Nayeri, Fan Yang, and Atef Z Elsherbeni. Reflectarray antennas: theory, designs, and applications. 2018.

[32] Olaf T Von Ramm and Stephen W Smith. Beam steering with linear arrays. *IEEE transactions on biomedical engineering*, (8):438–452, 1983.

[33] John Huang. Bandwidth study of microstrip reflectarray and a novel phased reflectarray concept. In *IEEE Antennas and Propagation Society International Symposium. 1995 Digest*, volume 1, pages 582–585. IEEE, 1995.

[34] ME Cooley, JF Walker, DG Gonzalez, and GE Pollon. Novel reflectarray element with variable phase characteristics. *IEE Proceedings-Microwaves, Antennas and Propagation*, 144(2):149–151, 1997.

[35] DM Pozar and TA Metzler. Analysis of a reflectarray antenna using microstrip patches of variable size. *Electronics Letters*, 29(8):657–658, 1993.

[36] Chunhui Han, Yunhua Zhang, and Qingshan Yang. A broadband reflectarray antenna using triple gapped rings with attached phase-delay lines. *IEEE Transactions on Antennas and Propagation*, 65(5):2713–2717, 2017.

[37] Eduardo Carrasco, Manuel Arrebola, Jose A Encinar, and Mariano Barba. Demonstration of a shaped beam reflectarray using aperture-coupled delay lines for lmds central station antenna. *IEEE transactions on antennas and propagation*, 56(10):3103–3111, 2008.

[38] John Huang and Ronald J Pogorzelski. A ka-band microstrip reflectarray with elements having variable rotation angles. *IEEE transactions on antennas and propagation*, 46(5):650–656, 1998.

[39] Chulmin Han, Christopher Rodenbeck, John Huang, and Kai Chang. Ac/ka dual frequency dual layer circularly polarized reflectarray antenna with microstrip ring elements. *IEEE Transactions on Antennas and Propagation*, 52(11):2871–2876, 2004.

[40] Daniel G Gonzalez, Gerald E Pollon, and Joel F Walker. Microwave phasing structures for electromagnetically emulating reflective surfaces and focusing elements of selected geometry, February 27 1990. US Patent 4,905,014.

[41] G Donzelli, A Vallecchi, F Capolino, and Alexander Schuchinsky. Metamaterial made of paired planar conductors: Particle resonances, phenomena and properties. *Metamaterials*, 3(1):10–27, 2009.

[42] Filippo Capolino, Andrea Vallecchi, and Matteo Albani. Equivalent transmission line model with a lumped x-circuit for a metalayer made of pairs of planar conductors. *IEEE transactions on antennas and propagation*, 61(2):852–861, 2012.

[43] A Vallecchi, A Schuchinsky, and F Capolino. Reconfigurable metasurface comprised of dogbone shaped conductor pairs. In *2015 IEEE International Symposium on Antennas and Propagation & USNC/URSI National Radio Science Meeting*, pages 1098–1099. IEEE, 2015.

[44] Andrea Vallecchi, Javier R De Luis, Filippo Capolino, and Franco De Flaviis. Low profile fully planar folded dipole antenna on a high impedance surface. *IEEE transactions on antennas and propagation*, 60(1):51–62, 2011.

[45] Shiji Pan, Eva Rajo Iglesias, and Filippo Capolino. Artificial magnetic conductor from a layer of dogbone-shaped conductors over a ground plane. In *2010 IEEE Antennas and Propagation Society International Symposium*, pages 1–4. IEEE, 2010.

[46] Georges A Deschamps. Microstrip microwave antennas. In *Proceedings of the Third Symposium on the USAF Antenna Research and Development Program, Oct*, pages 18–22, 1953.

[47] Warren L Stutzman and Gary A Thiele. *Antenna theory and design*. John Wiley & Sons, 2012.

[48] Constantine A Balanis. *Antenna theory: analysis and design*. John wiley & sons, 2015.